

UNCLASSIFIED

AD 431012

DEFENSE DOCUMENTATION CENTER

FOR

SCIENTIFIC AND TECHNICAL INFORMATION

CAMERON STATION, ALEXANDRIA, VIRGINIA



UNCLASSIFIED

NOTICE: When government or other drawings, specifications or other data are used for any purpose other than in connection with a definitely related government procurement operation, the U. S. Government thereby incurs no responsibility, nor any obligation whatsoever; and the fact that the Government may have formulated, furnished, or in any way supplied the said drawings, specifications, or other data is not to be regarded by implication or otherwise as in any manner licensing the holder or any other person or corporation, or conveying any rights or permission to manufacture, use or sell any patented invention that may in any way be related thereto.

64-9

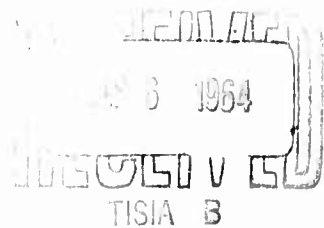
AMRL-TDR-62-140 (IV)

**RESEARCH ON SOUND PROPAGATION  
IN SOUND-ABSORBENT DUCTS  
WITH SUPERIMPOSED AIR STREAMS**

**VOLUME IV**

TECHNICAL DOCUMENTARY REPORT No. AMRL-TDR-62-140 (IV)

DECEMBER 1963



BIOPHYSICS LABORATORY  
6570th AEROSPACE MEDICAL RESEARCH LABORATORIES  
AEROSPACE MEDICAL DIVISION  
AIR FORCE SYSTEMS COMMAND  
WRIGHT-PATTERSON AIR FORCE BASE, OHIO

Contract Monitor: Robert G. Powell  
Project No. 7231, Task No. 723104

(Prepared under Contract No. AF 61(052)-112 by  
F. Mechel, P. Mertens, W. Schilz  
Physikalisches Institut der Universität Göttingen  
Göttingen, Germany)

431012  
CATALOGED BY DDC  
AS AD No. \_\_\_\_\_  
431012

## NOTICES

When US Government drawings, specifications, or other data are used for any purpose other than a definitely related government procurement operation, the government thereby incurs no responsibility nor any obligation whatsoever; and the fact that the government may have formulated, furnished, or in any way supplied the said drawings, specifications, or other data is not to be regarded by implication or otherwise, as in any manner licensing the holder or any other person or corporation, or conveying any rights or permission to manufacture, use, or sell any patented invention that may in any way be related thereto.

Qualified requesters may obtain copies from the Defense Documentation Center (DDC), Cameron Station, Alexandria, Virginia. Orders will be expedited if placed through the librarian or other person designated to request documents from DDC formerly ASTIA).

Do not return this copy. Retain or destroy.

Stock quantities available at Office of Technical Services, Department of Commerce, Washington 25, D. C. Price per copy is \$1.75.

### Change of Address

Organizations receiving reports via the 6570th Aerospace Medical Research Laboratories automatic mailing lists should submit the addressograph plate stamp on the report envelope or refer to the code number when corresponding about change of address.

## FOREWORD

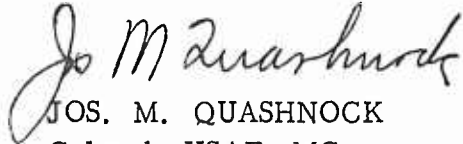
This report is Volume IV of a series of reports on sound propagation in sound-absorbent ducts with a superimposed air stream prepared by Göttingen University, Göttingen, Germany, for the Biodynamics and Bionics Division, Biophysics Laboratory, 6570th Aerospace Medical Research Laboratories, Aerospace Medical Division, under Contract AF 61(052)-112. The work was performed under Project 7231, "Biomechanics of Aerospace Operations," Task 723104, "Biodynamic Environments of Aerospace Flight Operations." Principal Investigators for Göttingen University were Dr. Erwin Meyer and Dr. Fridolin Mechel. Technical and administrative personnel monitoring this effort have included Dr. H. von Gierke, R. G. Powell, and J. N. Cole. Initial research on this program, resulting in the four volumes of this report, commenced in June 1958.

## ABSTRACT

This report, Volume IV, presents the results (1961-1962) of several studies of the interaction between air flow and airborne sound in a duct. Three projects are discussed: (1) Part A: The effects of various sound fields on the excitation of the boundary layer of a flat plate are discussed relative to the stagnation point and the boundary layer itself. Boundary layer distortions are shown to be a function of the sound signal and flow velocity. (2) Part B: The change in the cross-sectional distribution of the sound pressure in an absorbent duct with air flow is examined with respect to the shape of the velocity profile of the flow. Even for wavelengths greater than the boundary layer thickness the sound pressure increased at the absorbing walls. (3) Part C: The dependence of the acoustic radiation impedance of a tube orifice during flow conditions is investigated as a function of the flow velocity and turbulence level. Results show that as the flow increases the radiation impedance decreases.

## PUBLICATION REVIEW

This technical documentary report is approved.

  
JOS. M. QUASHNOCK  
Colonel, USAF, MC  
Chief, Biophysics Laboratory

## TABLE OF CONTENTS

	<u>Page</u>
INTRODUCTION.....	1
PART A    Investigations About the Effect of Acoustic Excitation on the Flow Boundary Layer in Air.....	3
I.        Experimental Set-up.....	3
II.       Boundary Layer Control at the Stagnation Point.....	4
III.      Effect of Pistonlike Vibrations of Part of the Test Plate on the Boundary Layer.....	18
IV.      Sound Radiated Through a Porous Plate.....	22
PART B    Sound Propagation in Ducts with Superimposed Air Flow	24
I.        Experimental Set-up. Rayleigh Absorber.....	24
II.       Sound Pressure Profiles.....	27
III.      Attenuation.....	30
IV.      Conclusions.....	32
PART C    Influence of Flow Through an Orifice on its Radiation Impedance.....	34
I.        Experimental Set-up.....	34
II.       Impedance Formula.....	35
III.      Preliminary Measurements.....	38
IV.      Impedance Measurements.....	42
V.       Measurement of the Reflection Coefficient of the Orifice with Increased Turbulence.....	46
VI.      Conclusions.....	49

## LIST OF ILLUSTRATIONS

<u>Figure</u>		<u>Page</u>
1	Experimental set-up.....	3
2	Areas of acoustic turbulence suppression and excitation as a function of the signal frequency $f_g$ and the Reynolds number.....	6
3	Shift of the transition point from laminar to turbulent flow as a function of the signal frequency $f_g$ . Parameter: Oscillatory velocity amplitude of the signal.	6
4	Turbulent velocity amplitudes $v_t$ with sound radiation as a function of signal frequency $f_g$ .....	8
5	Propagation exponent of the turbulent velocity amplitude $v_a$ with ( $a_g$ ) and without ( $a_n$ ) sound radiation vs. frequency	8
6	Comparison of the measured mean flow velocity $V$ at the leading edge of the test plate ( $x = -0.5$ mm) with the approximation formula.....	12
7	Measured phase profiles at the leading edge at the distances $x = -0.5$ mm (-o-o-) and $x = -1.5$ mm (- $\Delta$ - $\Delta$ -).	12
8	Velocity amplitude profiles of the oscillatory velocities of the fundamental wave and the first harmonic (y-components) compared with the approximate calculation. $x = -0.5$ mm.....	13
9	Oscillatory velocity $v$ at the leading edge for several phase angles. Excitation of eddies schematically.....	15
10	Oscillatory velocities of the boundary layer waves generated by two sound signals vs. axial distance from the leading edge. Signal amplitudes are shown as $f_1$ and $f_2$ .....	16
11	Spectra of the boundary layer disturbances with and without sound signals added.....	17



<u>Figure</u>	<u>Page</u>
12 Distribution of the measured frequencies of boundary layer waves generated by the vibrating ribbon (constant frequency 600 cps) and the variable sound signal with frequency $f_s$ .....	20
13 Suppression of the r. m. s. turbulent velocity oscillations by a sound signal as a function of axial position $x$ . ....	21
14 Spectra of the boundary layer disturbances of Figure 13 with and without sound signal for two positions.....	21
15 Shift of the transition point from laminar to turbulent boundary layer by a sound signal through the porous plate	23
16 Turbulent eruptions in the blow-out phases above the porous plate.....	23
17 Wall impedance of a Rayleigh absorber with finite thickness.....	26
18 Attenuation in the duct coated with (a) the Rayleigh absorber, and (b) a Rayleigh absorber covered with a porous foil.....	27
19 Sound pressure and flow velocity profiles for a duct with rigid walls.....	29
20 Sound pressure distribution in the duct with rigid walls at $V = 0$ and $V = 80$ m/sec. Averaged profiles.....	30
21 Sound pressure and flow velocity profiles in the sound absorbing duct.....	31
22 Sound pressure distribution in the sound absorbing duct at $V = 0$ and $V = 80$ m/sec. Averaged profiles.....	32
23 Reflection factors $r_M$ of the orifice in a baffle normalized with the theoretical value $r_0$ without flow vs. $ka$ .....	40
24 Normalized phase angle $\sigma = \psi / \pi$ of the reflection factor of the orifice in a baffle vs. $ka$ .....	41

<u>Figure</u>	<u>Page</u>
25 Normalized real part $F/\rho c_0$ of the radiation impedance of the orifice in a baffle vs. $ka$ .....	43
26 Normalized imaginary part $X/\rho c_0$ of the radiation impedance of the orifice in a baffle vs. $ka$ .....	44
27 Normalized real part of the radiation impedance of the unflanged orifice vs. $ka$ .....	45
28 Relative magnitude of the reflection coefficient of the orifice $r(ka, V_{\max})/r(ka, 0)$ vs. $ka$ . Grating No. 5.....	47
29 Magnitude of the reflection coefficient of the orifice $r_f(V_{\max})$ at $f = 1.2$ kcps for different gratings.....	50

LIST OF TABLES

<u>Number</u>	<u>Page</u>
I Average Turbulence Level in the Core as a Function of Grating Parameters.....	48
II Width of the Jet Behind the Orifice in cm.....	48

## LIST OF SYMBOLS

### PART A:

#### Frequencies:

$f_s$	Frequency of the acoustic signal
$f_w$	Frequency of the boundary layer wave
$f_a$	Center frequency of the filter for frequency analysis
$\Delta f$	Beat frequencies of boundary layer waves
$S$	Signal frequency of sound transducer
$B$	Frequency of vibrating ribbon
$\omega$	Angular frequency

#### Distances:

$x$	Coordinate in flow direction. Origin in stagnation point
$y$	Coordinate normal to plate surface. Origin at plate surface
$y'$	Coordinate normal to plate surface. Origin in stagnation point
$\delta^*$	Boundary displacement thickness
$S_0$	Elongation amplitude of sound signal
$S_1$	Elongation amplitude of sound signal
$S_2$	Elongation amplitude of sound signal

#### Velocities:

$V$	Local mean flow velocity
$V_\infty$	Mean flow velocity of undisturbed flow
$V_s$	Mean flow velocity near stagnation point

$v$	Oscillatory velocity
$v_t$	R. m. s. turbulent oscillatory velocity
$v_a$	Oscillatory velocity of boundary layer disturbances in a narrow frequency band

Other Quantities:

$A$	Elongation amplitude
$A_f$	Oscillatory velocity amplitude of a spectral component
$a_0, a_1$	Reference velocity amplitudes
$\alpha_n$	Propagation exponent of initial boundary layer disturbance
$\alpha_s$	Propagation exponent of boundary layer disturbance with superimposed sound signal
$\psi$	Phase angle
$\lambda$	Wavelength
$t$	Time

PART B:

$\rho$	Density of air
$c_0$	Adiabatic sound velocity
$W$	Acoustic energy flux through the duct
$I$	Acoustic intensity
$h$	Free height of the duct
$z$	Coordinate normal to absorber surface

PART C:

$\rho$	Density of air
$c_o$	Adiabatic sound velocity
$c_v$	Sound velocity in the tube with flow
$c_1$	Sound velocity in the downstream direction
$c_2$	Sound velocity in the upstream direction
$k_o$	Propagation exponent without flow
$k_1$	Propagation exponent for downstream propagation
$k_2$	Propagation exponent for upstream propagation
$\beta$	Phase constant
$\alpha$	Attenuation constant
$\lambda$	Wavelength
$V$	Flow velocity (average velocity)
$V'$	Axial flow velocity
$V_{av}$	Average flow velocity
$M = V/c_o$	Mach number
$p$	Sound pressure
$v$	Acoustical oscillatory velocity
$\underline{r} = r \cdot e^{j\psi}$	Reflection factor of the discharge orifice
$\underline{W} = R + jX$	Radiation impedance of the discharge orifice
$x$	Axial coordinate. Origin at the orifice
$j = (-1)^{1/2}$	

$d = p_{\min} / p_{\max}$	Standing wave ratio
$p_{\min}$	Sound pressure amplitude in pressure node
$p_{\max}$	Sound pressure amplitude in pressure antinode
$s$	Distance of nearest pressure node to discharge orifice
$Z_o = \rho c_o$	Characteristic impedance
$f$	Frequency
$\omega$	Angular frequency
$a$	Inner radius of measuring tube
$\sigma = \psi / \pi$	Normalized phase angle of reflection factor
$r_o$	Magnitude of reflection factor without flow
$r_M$	Magnitude of reflection factor at flow with Mach number $M$
$A$	Empirical proportionality constant
$r(f, V_{\max})$	Magnitude of the reflection coefficient of the orifice as a function of $f$ and $V_{\max}$
$r_f(V_{\max})$	Magnitude of the reflect coefficient of the orifice as a function of $V_{\max}$ at constant $f$

## INTRODUCTION

### PART A:

The purpose of the measurements reported in this part of the present report was to obtain information as to how the flow boundary layer of a flat plate can be influenced by sound fields or by oscillatory movements of parts of the plate. A point of special interest was the transition from laminar to turbulent flow.

Two kinds of boundary layer control were distinguished by these tests. The first was obtained by radiating a sound field into the flow prior to the development of the boundary layer at the leading edge of the plate, while the second was by the introduction of oscillatory movements of a downstream section of the plate. These oscillatory movements on their part can be either the pistonlike vibrations of a section of the test plate together with the radiated sound field, or it can be the sound wave radiated into the boundary layer of one side of the test plate through a porous, non-vibrating section of the test plate.

In the following report three kinds of oscillatory movements of the air in the boundary layer are to be discerned, viz. the movement in the acoustic wave, the periodic movements in the boundary layer wave, and the random movements generated by the turbulence. The decision as to whether a periodic oscillation belongs to a sound wave or to a boundary layer wave can be easily made by a measurement of the wavelength of the oscillation.

### PART B:

In former investigations (ref. 3) we measured the change of the sound attenuation in an absorbing duct caused by an air flow through the duct. The following influences of the flow on the sound attenuation could be discerned: a) convection of the sound wave by the flow, b) change of the sound pressure profile in the duct due to the change of the wavenumbers, c) change of the sound pressure profile in the duct due to the mean flow velocity profile, d) nonlinear variation of the wall impedance of the absorber, e) scattering of sound by the turbulence of the flow.

The effects under a) and b) could be described by a simple theory (ref. 2) in which the flow velocity was assumed to be constant over the cross section of the duct. Reported upon in this section are preliminary measurements taken to show the influence of the curved, mean flow velocity profile on the sound attenuation. From these measurements the necessary information shall be collected for the development of a theory of the sound attenuation in absorbing ducts with air flow, taking into account the curvature of the flow velocity profile.

The behavior of typical sound absorbers in a flow shall be investigated in future measurements.

PART C:

The measurements reported in this part are the initial results of an investigation which shall procure data about the influence of an air outflow through an orifice on the acoustic radiation impedance of that orifice. The object of these investigations is to find out which quantities of the flow velocity field behind the orifice affected the acoustic radiation impedance.

The radiation impedance is measured by the method of the impedance tube. Since the reflection coefficient at the orifice is near to unity the signal-to-noise ratio must be great enough for this method. That is why the flow velocities are restricted to values below about 160 m/sec.



## PART A

### INVESTIGATIONS ABOUT THE EFFECT OF ACOUSTIC EXCITATION ON THE FLOW BOUNDARY LAYER IN AIR

#### I. Experimental Set-up

In a previous volume, (ref. 3) measurements were reported concerning the effect of acoustic excitation on the flow boundary layer. The signal frequency in those measurements was 12.4 kcps. For similar tests the signal frequency and flow velocity have been extended to a greater range. In the new experimental set-up an electro-dynamical driving system is used for the generation of the sound signal with frequencies between 0.1 and about 5 kcps. Furthermore, means were procured to generate monochromatic boundary layer waves of variable frequency. Figure 1 represents a schematical view of the experimental set-up. The test section of the measuring duct has a free cross-sectional area at the inlet of  $10 \times 10 \text{ cm}^2$ . The free height behind the leading edge of the test plate is 8 cm. The air outlet through the branch below the test plate can be regulated. By this regulation the level of the flow disturbances at the stagnation point of the test plate can be controlled. This provides the possibility to preset the rate of the development of the boundary layer above the plate.

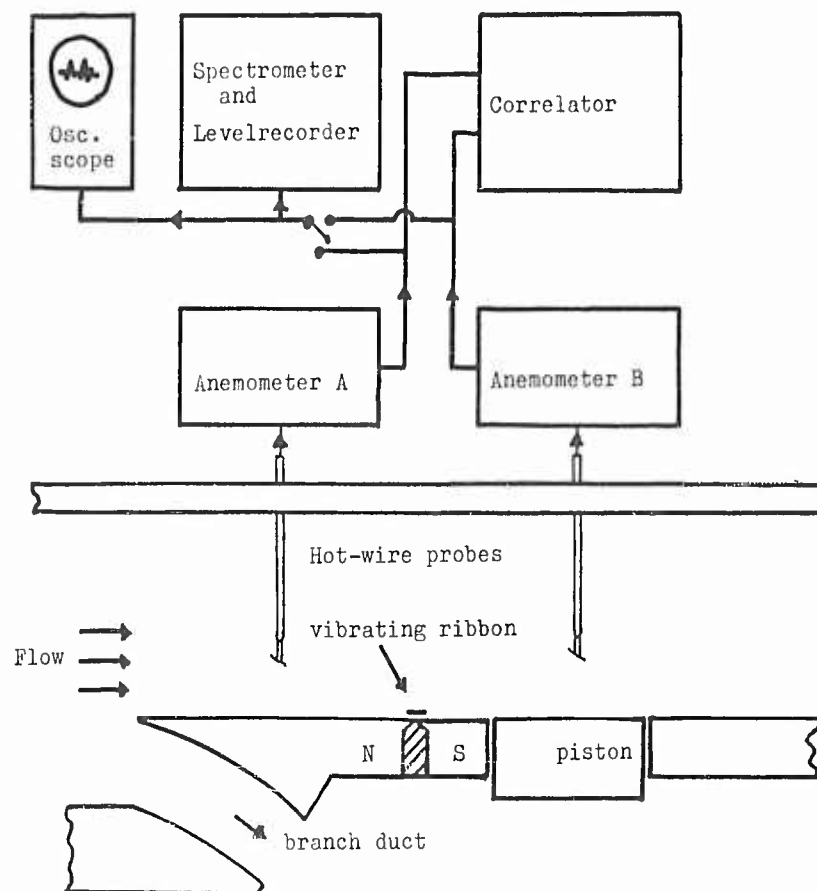


Figure 1 -  
Experimental Set-up

The excitation of monochromatic boundary layer waves is done by a thin metallic ribbon ( $0.01 \times 0.35 \text{ mm}^2$ ) stretched across the test plate within the boundary layer in a distance of 7 cm behind the leading edge of the test plate. The ribbon is placed in the stray field of a permanent magnet in the test plate. It can be excited electro-dynamically to vibrations normal to the plate surface. By these vibrations boundary layer waves are generated in the otherwise undisturbed boundary layer (ref. 7). Behind the vibrating ribbon different sound sources (pistonlike vibrating membranes, porous plates in front of loudspeakers) can be inserted evenly into the test plate. For other measurements sound is radiated into the branch duct below the test plate.

## II. Boundary Layer Control at the Stagnation Point

### II.1. Sound Induced on the Test Plate -

The object of the measurements reported in this section is the effect of a sound field on the boundary layer at the stagnation point of a plate. For this purpose the disturbance level at the stagnation point without signal was adjusted by choking of the branch duct to such a height that the boundary layer above the test plate became turbulent at a distance of about 15 cm from the leading edge. The sound generator is a flat, rigid oscillator inserted smoothly into the surface of the test plate. It works in the frequency range between 0.1 and 3.5 kcps. At a fixed station above the test plate the change of the disturbance level in the boundary layer was measured as a function of the sound signal. Variable parameters were signal frequency and signal intensity, flow velocity and initial disturbance level at the leading edge. For these measurements the initial disturbance level is adjusted to yield single turbulent spots at the position of the measuring probe in the no-signal condition.

For each flow velocity the effect of the acoustic signal on the boundary layer shows a strong frequency dependence. Three frequency ranges can be discerned in these measurements:

- 1) low frequencies: no interaction,
- 2) medium frequencies: increase of the boundary layer disturbances,
- 3) high frequencies: suppression of the boundary layer disturbances.

The increase of the disturbance level by the sound field finally leads to fully developed turbulence, whereas in the case of suppression of the disturbances the initial turbulent spots vanish absolutely. The strength of the excitation or suppression is dependent not only on the signal frequency but also on the amplitude of the sound signal and on the initial disturbance level. The frequency limits of the above mentioned frequency ranges, however, are virtually independent from the initial disturbance level and the signal amplitude.

In Fig. 2 these frequency ranges are shown. The abscissa is the Reynolds number corresponding to the boundary layer displacement thickness. The values of the abscissa in Fig. 2 correspond to flow velocities between 10 and 30 m/sec. The ordinate is the frequency of the sound signal. The position of the measuring probe was at about 20 cm behind the leading edge. The oscillatory velocity amplitude of the oscillator surface was in the order of magnitude of 1 cm/sec.

With increasing flow velocities the boundary layer becomes more and more sensitive with respect to induced distortions. Therefore, smaller and smaller signal amplitudes are sufficient for an increase of the disturbance level. For the suppression of the disturbances, on the other hand, greater and greater signal amplitudes are necessary. With increasing flow velocity the width of the excitation range is increased and is shifted towards higher frequencies. With the exception of these remarks the behavior is virtually the same for each flow velocity. Therefore, the following measurements could be restricted to one flow velocity only.

## II. 2. Sound Induced in Branch Duct -

During the above measurements it became evident that the interaction between the sound field and the boundary layer is located at the leading edge of the test plate. A further series of measurements was made for a detailed investigation of this effect. In these tests the sound signal was radiated into the branch duct below the test plate and the development of the disturbances generated at the leading edge was traced along the upper surface of the test plate. The branch duct was choked to a degree that the transition point from laminar to turbulent boundary layer without sound signal was at  $x = 10$  cm ( $x$  is the distance from the leading edge). By the sound signal, boundary layer waves with the frequency of the sound signal are generated at the leading edge. Depending on the frequency they are either damped out or increased during propagation. With a flow velocity of 10 m/sec a sound signal with a frequency between 1.0 and 1.8 kcps has an exciting effect. This was indicated by the following measurements:

### a) Shift of the transition point -

In Fig. 3 the position of the transition point is plotted as a function of the signal frequency with the signal amplitude as parameter. The oscillatory velocity amplitudes of the parameter are measured at the leading edge. With the greater amplitude (full line) the transition point is shifted in the downstream direction for frequencies above 1.8 kcps. The boundary layer is stabilized. In the maximum of destabilization the transition point is shifted in the upstream direction nearly to the leading edge.

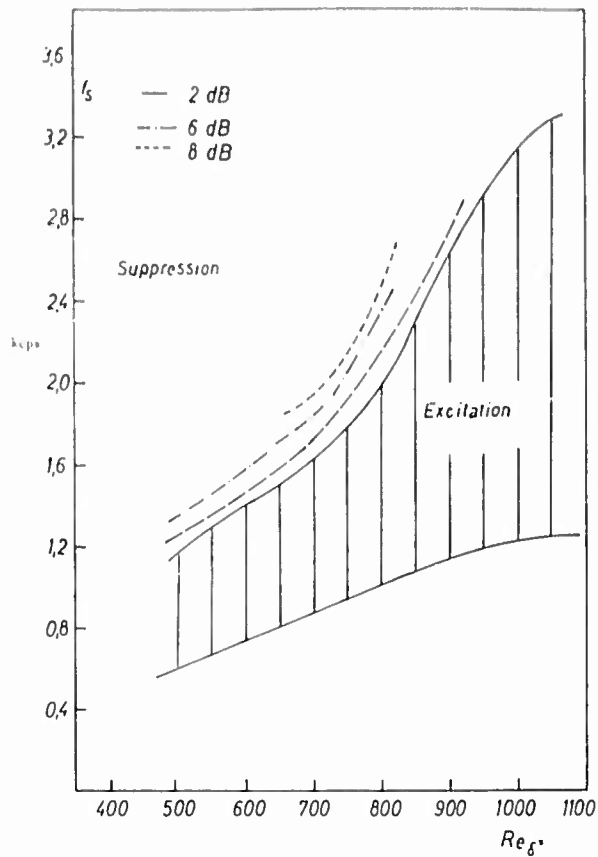


Figure 2 - Areas of acoustic turbulence suppression and excitation as a function of the signal frequency  $f_s$  and the Reynolds number.

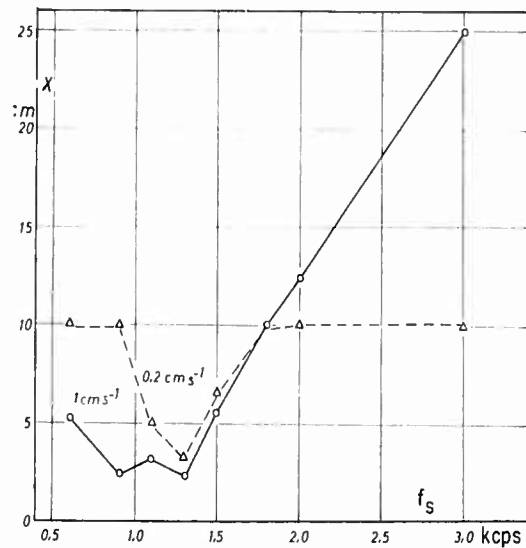


Figure 3 - Shift of the transition point from laminar to turbulent flow as a function of the signal frequency  $f_s$ .  
Parameter: Oscillatory velocity amplitude of the signal.

b) Change of the disturbance level -

In Fig. 4 the disturbance level at a constant measuring position ( $x = 10$  cm) is represented. The oscillatory velocity amplitude of the signal at the leading edge is about 0.3 cm/sec. The dashed line is the spectrum of the boundary layer disturbance without sound signal. The full line is the broadband r. m. s. disturbance level with superimposed sound signal as a function of signal frequency. At 1.3 kcps signal frequency a distinct maximum of excitation can be seen. Above 1.8 kcps suppression of the boundary layer disturbances up to an amount of 20 dB takes place.

c) Change of the propagation exponent -

For the individual frequency components of the boundary layer disturbances the propagation exponent  $\alpha$  of the amplitudes  $A_f$  was measured with and without sound signal. The amplitudes can be represented by

$$A_f = a_0 e^{\alpha_n x} \quad \text{without sound signal}$$

$$A_f = a_1 e^{\alpha_s x} \quad \text{with sound signal}$$

In Fig. 5 the measurement values of  $\alpha_n$  and of  $\alpha_s$  in dB/cm are plotted vs. the filter frequency in the no-signal measurement and vs. the signal frequency in the measurement with the sound signal radiated. The oscillatory velocity amplitude generated by the sound signal at the position  $x=0/y'=1$  mm ( $x=0/y'=0$  are the coordinates of the stagnation point) is for all frequencies about 0.3 cm/sec.

Fig. 5 shows that the propagation exponent of the boundary layer waves is increased in the frequency range of excitation. At low frequencies it remains nearly unchanged. At high frequencies, however, it is reduced to very small values. The difference  $\alpha_s - \alpha_n$  reveals the instability ( $\alpha_s - \alpha_n > 0$ ) or the stability ( $\alpha_s - \alpha_n < 0$ ) of the boundary layer waves generated at the leading edge. According to the theory by Tollmien and Schlichting (ref. 5), both of them are determined by the frequency and the Reynolds number. From Fig. 5 the following relations can be seen:

$$\alpha_s - \alpha_n < 0 \quad \text{for } f_s < 1 \text{ kcps and } f_s > 1.8 \text{ kcps}$$

$$\alpha_s - \alpha_n > 0 \quad \text{for } 1 \text{ kcps} < f_s < 1.8 \text{ kcps.}$$

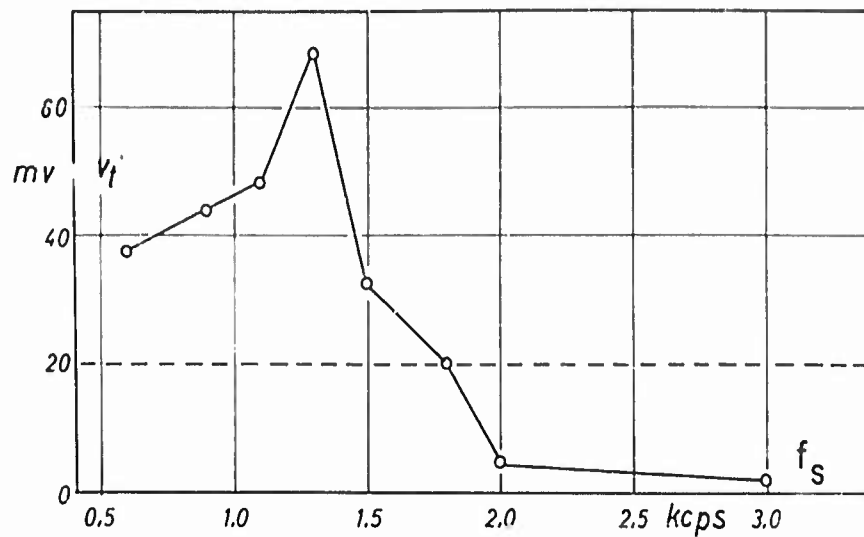


Figure 4 - Turbulent velocity amplitudes  $v_t$  with sound radiation as a function of signal frequency  $f_s$ .

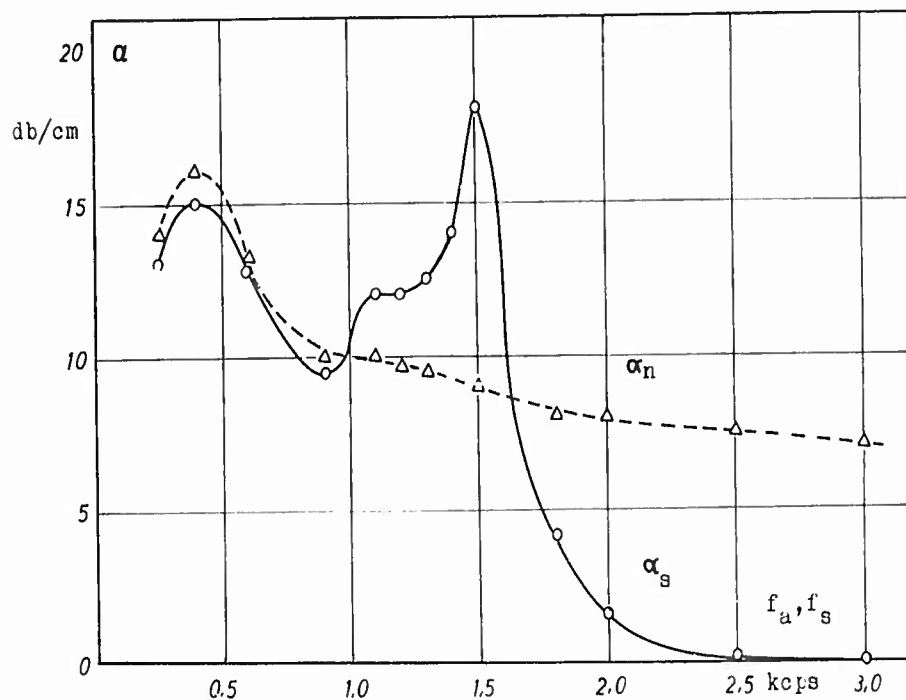


Figure 5 - Propagation exponent of the turbulent velocity amplitude  $v_a$  with ( $\alpha_s$ ) and without ( $\alpha_n$ ) sound radiation vs. frequency.

### II. 3. Mechanism of Excitation

The following measurements were taken to show the mechanism of the excitation of the boundary layer waves at the leading edge. The leading edge was rounded with a radius of curvature of 1 mm. The sound signal again is radiated into the branch duct below the test plate. The oscillatory velocity in the boundary layer behind the leading edge is caused by a super-position of two waves with different phase velocities. By evaluating the measurement of the amplitude distribution in the x-direction, of the phases and of the correlation coefficient, it can be seen that the two waves are a sound wave and a boundary layer wave respectively. The Reynolds number near the leading edge in these measurements was so small that the boundary layer waves always were damped out. With a flow velocity  $V_{\infty} = 10$  m/sec the following values of the wavelength  $\lambda$  of the boundary layer wave, its phase velocity  $\lambda f$  and its attenuation per wavelength  $\alpha \lambda$  were measured:

f	(kcps)	0.5	0.9	1.1	1.3	1.5	2.0	2.5
$\lambda f$	(m/sec)	4.45	5.3	5.5	5.85	5.6	6.0	6.25
$\lambda$	(cm)	0.89	0.59	0.5	0.45	0.37	0.3	0.25
$\alpha \lambda$	(dB)	-2.24	-1.33	-1.17	-1.9	-2.46	-2.5	-3.15

The maximum of  $\alpha \lambda$  is at  $f_s = 1.1$  kcps.

In another set of measurements the velocity field at the leading edge was studied. For this purpose the spatial distribution of the amplitude, of the phase and of the mean flow velocity were in the immediate vicinity of the leading edge. For technical reasons the measuring position was at a distance of 0.5 mm from the stagnation point. There the mean flow velocity is

$$V_s (x=-0.5/y'=0) = 0.5 \cdot V_{\infty} = 4 \text{ m/sec.}$$

The measured flow velocity profile can be approximated by

$$V = V_{\infty} \left( 1 - \frac{V_s}{V_{\infty}} \frac{1}{1 + y'^2} \right).$$

With this representation and with the assumption that the oscillatory velocities of the sound field normal to the direction of the incoming flow move the mean flow velocity profile as a total, i. e. without change of the shape of the profile, an approximate evaluation of the resulting oscillatory velocities and of their phase distribution is possible.

If the elongation amplitude of the sound field is

$$A = S_0 \sin \omega t,$$

$$\omega = 2\pi f,$$

the local flow velocity is

$$V + v = V_\infty \left[ 1 - \frac{V_s}{V_\infty} \frac{1}{1 + (y' + S_0 \sin \omega t)^2} \right]$$

$$= V_\infty \left[ 1 - \frac{V_s}{V_\infty (1 + y'^2 + S_0^2)} \frac{1}{1 + \frac{2y'S_0 \sin \omega t - (S_0^2/2) \cos 2\omega t}{1 + y'^2 + S_0^2/2}} \right]$$

Expansion in a power series with  $S_0 \ll 1$  leads to

$$V + v = V_\infty \left[ 1 - \frac{1}{2(1 + y'^2)} \left( 1 - \frac{S_0}{2} \frac{4y' \sin \omega t - S_0 \cos 2\omega t}{1 + y'^2} \right) \right]$$

which contains the oscillatory velocities of the fundamental wave and of the first harmonic

$$v = \frac{V_\infty S_0}{4(1 + y'^2)^2} (4y' \sin \omega t - S_0 \cos 2\omega t).$$

The amplitude  $S_0$  was determined from the experiments by the ratio of the amplitudes of the fundamental wave and of the first harmonic at  $y' = 1$  mm. This ratio was 35 dB which results in

$$S_0 = 0.07 \text{ mm.}$$



#### II.4. Theoretical and Experimental Comparisons

The comparison between the calculated approximation and the experimental results shows a good agreement. In Fig. 6 the measured mean flow velocity profile is compared with the profile from the approximation formula. In Fig. 7 the phase profiles measured in two distances from the stagnation point are represented. The approximate calculation shows a shift in phase of  $\pi$  when crossing the plane  $y'=0$ . In the immediate vicinity of the stagnation point the calculation yields no constant phase since there the amplitudes of the fundamental wave and of the first harmonic are of the same magnitude. The measurement at  $x = -0.5$  mm yields the same phase curve. In addition to the transition from  $-\pi/2$  to  $+\pi/2$  a spatial oscillation of the phase is superimposed which can be interpreted by the superposition of an eddy. The correlation coefficient has virtually the same profile as the phase.

The second curve in Fig. 7 is the measured phase profile in the distance  $x = -1.5$  mm. There too a phase shift of about  $\pi$  is connected with the crossing of the stagnation line. The oscillation of the phase profile is much smaller, however. This too can be interpreted by the just mentioned eddy. At  $x = -0.5$  mm the eddy is intersected in the center (phase shift of  $\pi$ ) whereas at  $x = -1.5$  mm it is intersected outside its center. This is illustrated by the sketch added in Fig. 7.

The approximate calculation yields an amplitude profile for the oscillatory velocity of the frequency  $f$  and the existence of the harmonic  $2f$  in the vicinity of the stagnation point. The measured profiles of these two components are compared with the calculated ones in Fig. 8. There only the branches for positive values of  $y'$  are plotted. For negative values of  $y'$  the curve of the fundamental wave is symmetric with respect to the origin, the curve for the first harmonic is symmetrical with respect to the ordinate. The ordinate value of 0 dB corresponds to an amplitude of 1 mm/sec. The fundamental wave shows a good agreement between the calculated and the measured curves near  $y' = 0$ . The calculated curve of the first harmonic reflects the course of the measured curve. In connection with this statement it shall be mentioned that the harmonic is about 40 dB below the fundamental wave and that the sound generator itself radiates harmonics. In the evaluation a harmonic content of the generator of 1 percent was taken into account.

The agreement between measurement and calculation justifies the use of our formula for the calculation of the local flow velocity field near the stagnation point. It comes out that in the vicinity of the stagnation point rotary fields are generated by which boundary layer waves can be excited.

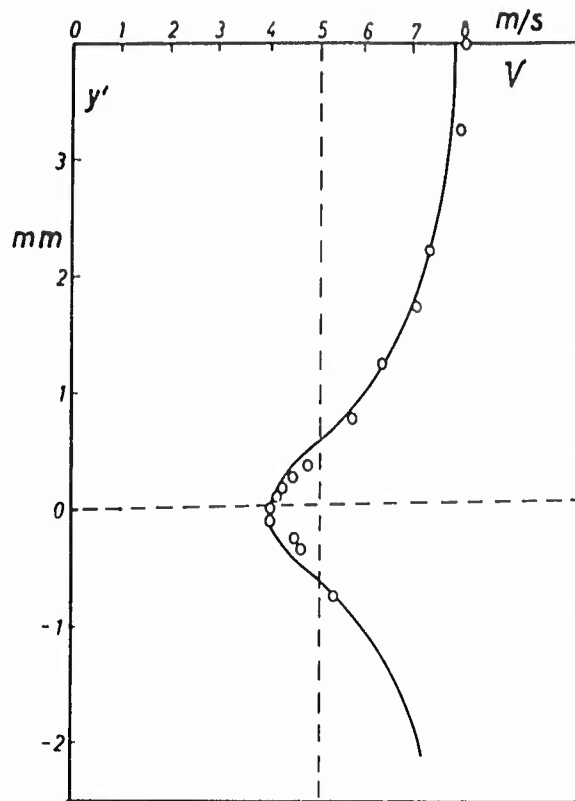


Figure 6 - Comparison of the measured mean flow velocity  $V$  at the leading edge of the test plate ( $x = -0.5$  mm) with the approximation formula.

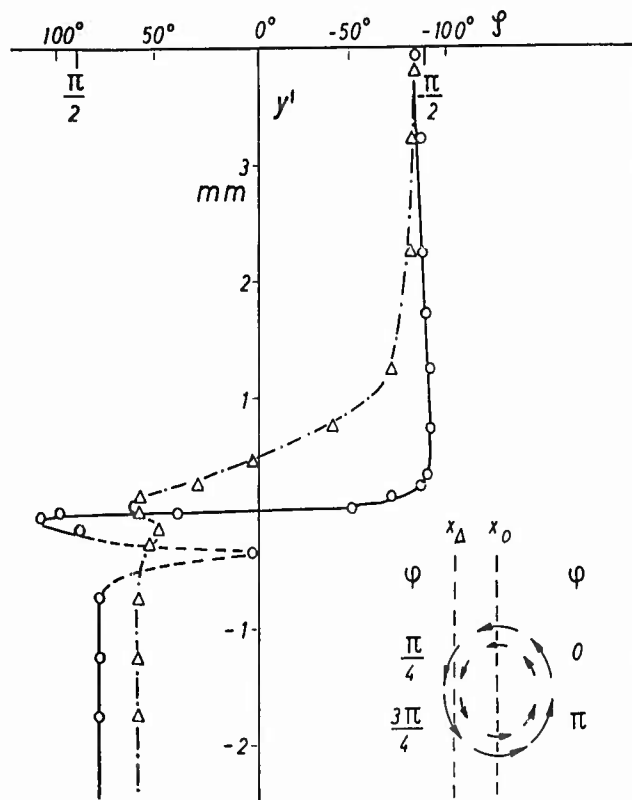


Figure 7 - Measured phase profiles at the leading edge at the distances  $x = -0.5$  mm (-o-o-) and  $x = -1.5$  mm (-Δ-Δ-).

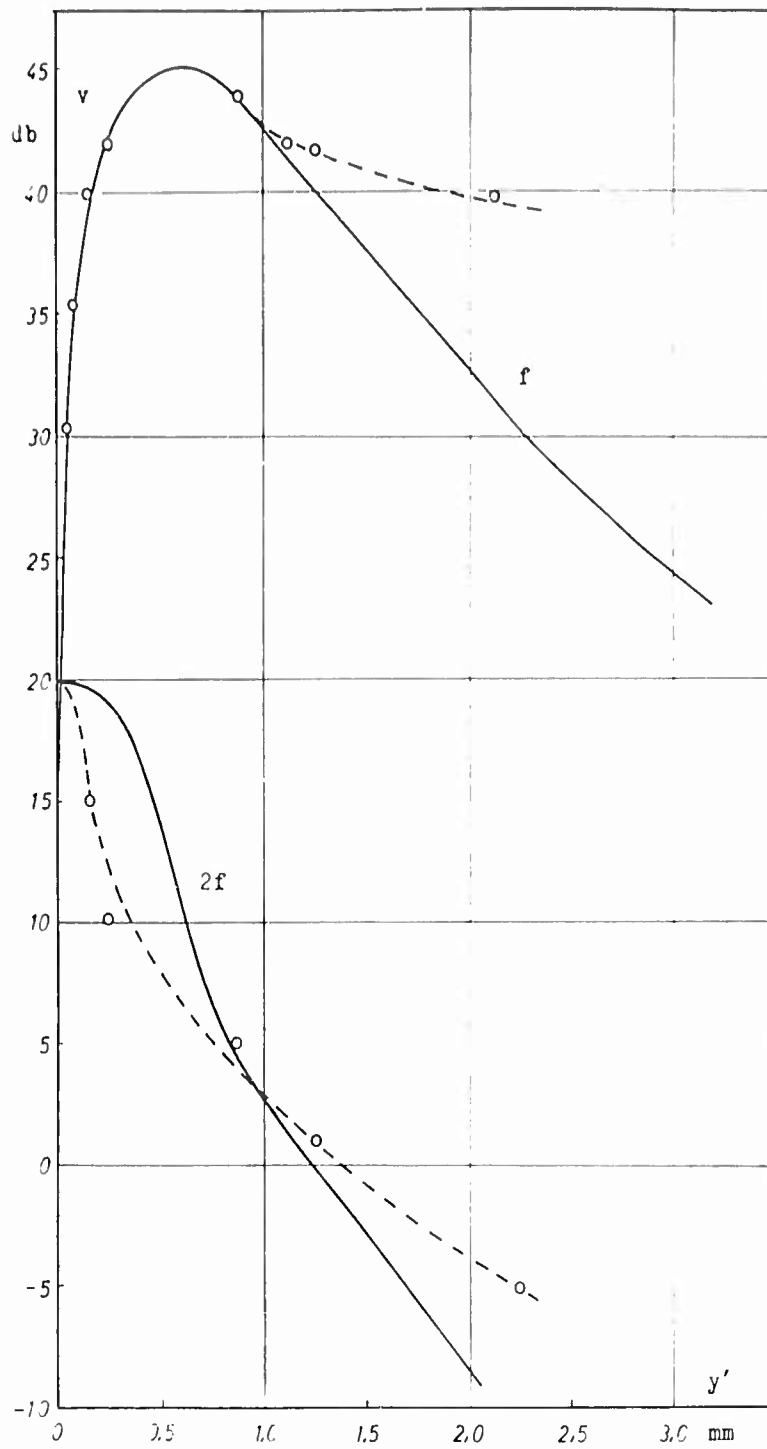


Figure 8 - Velocity amplitude profiles of the oscillatory velocities of the fundamental wave and the first harmonic (y-components) compared with the approximate calculation.  $x = -0.5$  mm.

The calculated velocity amplitudes for different phases  $\omega t$  of the sound field near the stagnation point are plotted in Fig. 9. In the interval between  $\omega t = \pi/4$  to  $\pi/2$  a negative rotary field is generated with the center of rotation at  $y' = -0.06$  mm. A corresponding positive rotary field is generated during the interval between  $5\pi/4$  to  $3\pi/2$  with the center of rotation at  $y' = +0.06$  mm.

If this rotary field generates eddies the rate of the generation is  $2f$ . By the movement of the center of rotation normal to the plane  $y' = 0$ , however, successive eddies are shed to the opposite sides of the test plate. Thus, on each side of the test plate the repetition rate of the eddies is  $f$ . This behavior is indicated in the sketch of Fig. 9. By this, the generation of a boundary layer wave of the frequency  $f$  can be explained.

#### II. 5. Effects of Sum and Difference Frequencies on the Boundary Layer Disturbances -

The considerations developed above explain the generation of boundary layer waves by a sound field at the stagnation point of the test plate. The measurements reported in previous sections indicate that these boundary layer waves in their turn give rise to the excitation or to the suppression of the initial boundary layer disturbances. For the explanation of these effects a mechanism of interaction between the boundary layer waves generated by the sound field and the initial boundary layer disturbances must be assumed.

This mechanism was investigated first for the case of two different sound signals -  $S_1 \sin \omega_1 t$  and  $S_2 \sin \omega_2 t$  - at the leading edge. The expression for the local velocity thus becomes:

$$V + v = V_\infty \left[ 1 - \frac{V_s}{V_\infty} \frac{1}{1 + (y' + S_1 \sin \omega_1 t + S_2 \sin \omega_2 t)^2} \right]$$

By the same method as above the resulting oscillatory velocity is:

$$v = V_\infty \frac{V_s / V_\infty}{(1 + y'^2)^2} \left[ \begin{aligned} &2y'(S_1 \sin \omega_1 t + S_2 \sin \omega_2 t) \\ &- 0.5 (S_1^2 \cos 2\omega_1 t + S_2^2 \cos 2\omega_2 t) \\ &+ S_1 S_2 (\cos(\omega_1 - \omega_2)t - \cos(\omega_1 + \omega_2)t) \end{aligned} \right].$$

Besides the two fundamental waves and their harmonics, waves with the sum and the difference frequencies are generated.

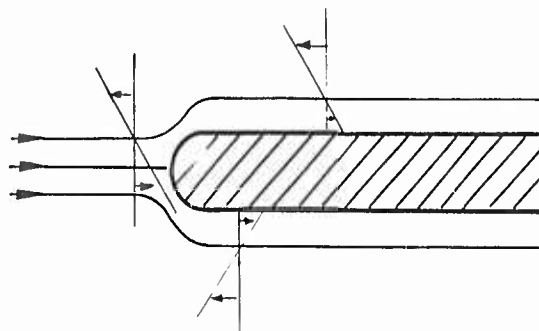
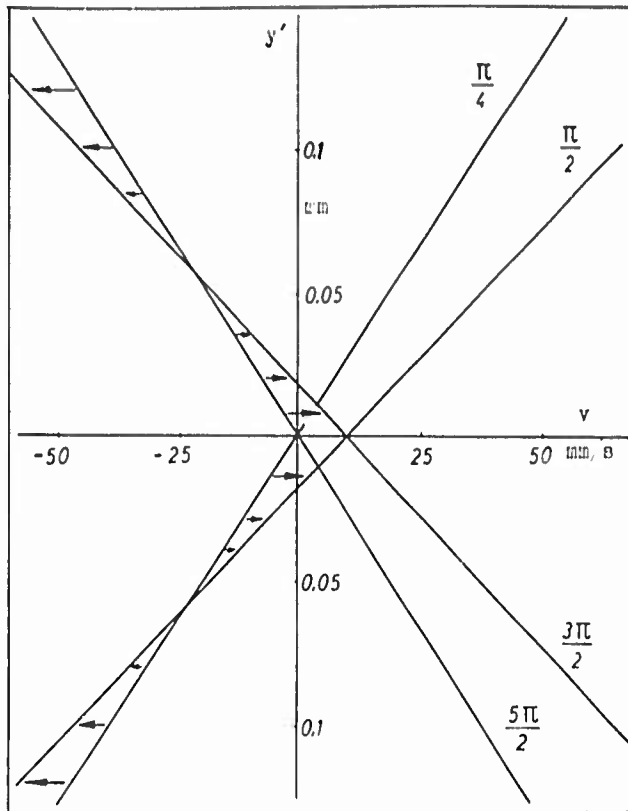


Figure 9 - Oscillatory velocity  $v$  at the leading edge for several phase angles. Excitation of eddies schematically.

In the measurements the two frequencies were  $f_1 = 1.23$  kcps and  $f_2 = 1.84$  kcps. The beat frequency  $f_2 - f_1$  is in the frequency range of excitation. If the amplitudes of the two input signals are changed within a 40 dB range each, the amplitude of the beat frequency oscillation is proportional to the product of the two input signals, as it should be from the equation.

Normally the amplitudes of the newly generated boundary layer waves of higher frequencies than the beat frequency are small (from the beginning and they become even smaller by attenuation) so that it is difficult to measure them. In order to increase them for a small distance a short section of increasing pressure was inserted behind the leading edge. By this means, all boundary layer disturbances are increased along this short distance. In Fig. 10 the amplitudes of the boundary layer waves of different frequencies generated by the two sound signals are plotted vs. distance from the leading edge. For the waves of the frequencies  $f_1$  and  $f_2$  only the initial amplitudes are indicated. They are at the position  $x=0/y'=0.5$  mm  $A(f_1) = 1.5$  cm/sec and  $A(f_2) = 2.9$  cm/sec.

Fig. 10 shows that all boundary layer waves with the exception of that with the frequency  $f_2 - f_1$  are damped behind the section with increasing pressure. In the table in Fig. 10 the measured frequencies of the boundary layer waves are compared with those calculated from the frequencies of the two input signals.

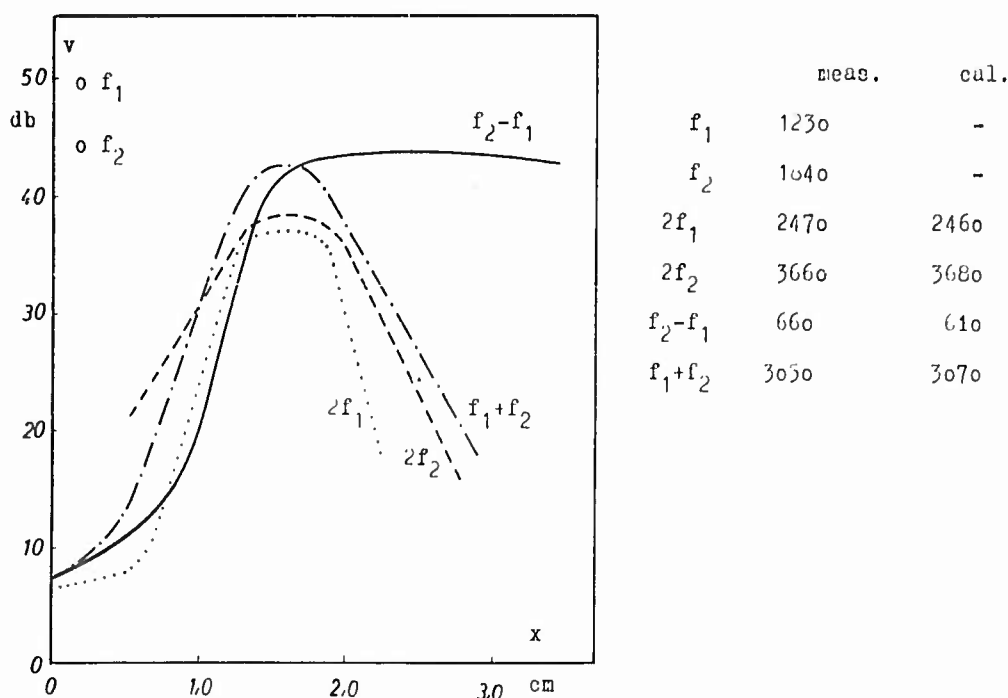


Figure 10 - Oscillatory velocities of the boundary layer waves generated by two sound signals vs. axial distance from the leading edge. Signal amplitudes are shown as  $f_1$  and  $f_2$ .

## II. 6. Boundary Layer Spectrum -

If the initial boundary layer disturbances are excited or suppressed by the sound signal, the signal has to interact with a broad turbulent spectrum. This spectrum of the initial boundary layer disturbances due to disturbances of the incoming flow reveals a distinct maximum at about 70 cps if measured 4 cm behind the leading edge, i. e. at a position where the boundary layer is still laminar. This maximum of the spectrum is about 30 dB higher than the components above 2 kcps.

If a sound signal is radiated with a frequency within the range of the disturbance excitation, the spectral analysis of the resulting disturbances shows that the sides of the peak at the signal frequency are lifted, (see Fig. 11). There are maxima on the sides of the signal peak at  $f_s \pm 70$  cps ( $f_s$  = signal frequency, measuring accuracy 20 cps). These maxima are greatest if the signal frequency  $f_s$  is in the center of the excitation range. If, however, the signal frequency is in the frequency range of disturbance suppression, for example at  $f_s = 3.12$  kcps, the signal peak is unchanged and the total spectrum of the resulting boundary layer disturbance is lowered.

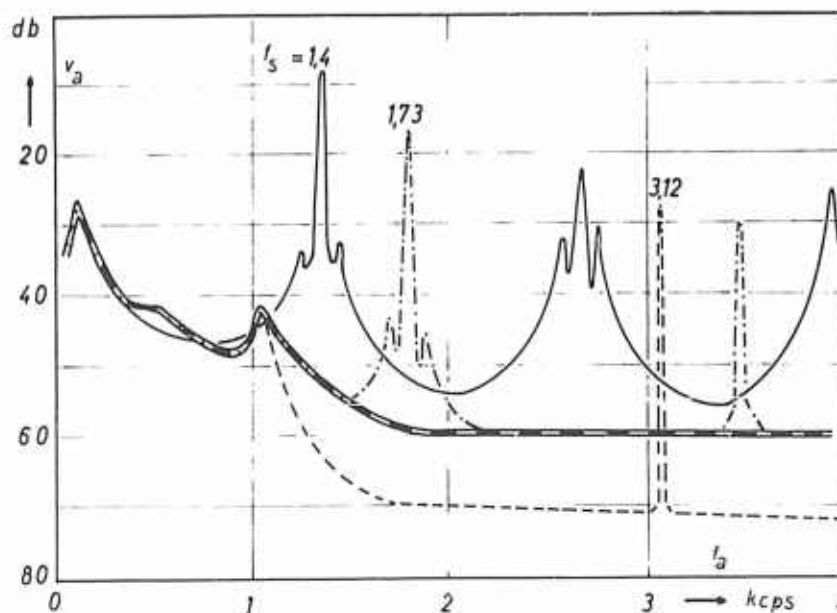


Figure 11 - Spectra of the boundary layer disturbances with and without sound signals added.

These findings can be explained by the statement that the sound signal is modulated with the initial disturbances. Then the sum and difference frequencies are generated. This gives rise to the maxima on the sides of the signal peaks in a distance of about 70 cps from the signal frequency. By this

modulation more oscillatory energy is transposed into the excitation frequency range, if the sound signal is in the excitation range. If a high frequency sound signal is radiated, the beat frequencies are also damped out very soon. The disturbances are not increased. Whereas for a low frequency sound signal of high intensity the sides of the signal peak itself are not raised, the slopes of the higher harmonics of the signal which are in the excitation range again are emphasized. This is the reason for the excitation of the boundary layer disturbances with high intensity signals with frequencies below 1 kcps, which can be seen in Fig. 3.

### III. Effect of Pistonlike Vibrations of Part of the Test Plate on the Boundary Layer

Another kind of acoustic effect on the boundary layer of a flat plate is brought about by pistonlike vibrations of a part of the test plate normal to its surface. The transducer is smoothly inserted into the test plate. The boundary layer waves which shall be affected by the transducer oscillations are generated by the vibrating ribbon.

If there are no initial disturbances in the boundary layer only sound waves are measured above the transducer. The oscillatory velocities drop very rapidly on the sides beyond the transducer. Boundary layer waves are not generated. Above the transducer the amplitude of the oscillatory velocities also decreases very rapidly in the y-direction as shown:

y (mm)	0.25	0.5	1.0	2.0
A (mm/sec)	62.5	29.0	22.0	12.0

The oscillatory velocity amplitude measured by the hot-wire anemometer is proportional to the first derivative of the mean flow velocity profile:

$$A(y) = A_0 \frac{dV}{dy}$$

The relationship indicates that the mean flow velocity profile is moved as a whole by the oscillatory amplitude of the transducer which is normal to the flow direction. This effect is the same as that with the profile in the stagnation point.

Since the radiation field of the transducer itself generates no boundary layer waves, a strong interaction of this radiation field with the boundary layer waves which travel through the field is measured. As a consequence of this interaction a number of new boundary layer waves are generated, the



frequencies of which,  $\Delta f$ , can be represented as the difference between multiples of the signal frequency,  $S$ , and multiples of the vibrating ribbon frequency,  $B$ :

$$\Delta f = |nS - mB|, \quad n, m = 1, 2, 3,$$

Difference frequencies up to the third order ( $3S-3B$ ) were observed. In no case were boundary layer waves observed with a frequency equal to the sum of the two frequencies.

Fig. 12 is a representation of all observed boundary layer wave frequencies. The frequency of the vibrating ribbon,  $B$ , was held constant at 600 cps. The abscissa is the frequency of the pistonlike transducer. The ordinate is the frequency of the newly generated boundary layer waves. The lines in this graph are the possible difference frequencies. From the density of the measured points in Fig. 12 it can be seen that the frequencies  $|S - B|$  and  $|S - 2B|$  are most often excited. If the frequency  $B$  of the ribbon is changed, similar distributions are obtained.

The hot-wire anemometer cannot distinguish between oscillatory velocities associated with either a sound wave or a boundary layer wave. By correlation measurements, however, it could be shown, that the waves with the difference frequencies are boundary layer waves. The sound signal generates no boundary layer wave of its own frequency. The intensity of the difference frequency boundary layer waves depends strongly on the intensity of both the sound signal and the initial boundary layer wave. A general observation is the decrease of the intensity of the difference waves with increasing frequency.

The boundary layer waves with the difference frequencies are responsible for the stability of the boundary layer. Whenever there are such boundary layer waves in the instable frequency range, the boundary layer disturbances of the incoming flow are increased. Suppression of the boundary layer disturbances was found to be correlated with difference waves only in the frequency range below the instable range.

In Fig. 13 is shown the development of a boundary layer disturbance which is generated by a 220 cps boundary layer wave. At  $x = 40$  cm the boundary layer becomes turbulent. If a sound signal of 380 cps is added, the intensity of the disturbance is lowered. At the positions  $x = 30$  cm and  $x = 46$  cm a frequency analysis of the disturbances was made. It is plotted in Fig. 14. At  $x = 30$  cm, without sound signal, only the line at the frequency  $f_1$  of the initial boundary layer wave is seen. With added sound signal the lines of the signal ( $f_2$ ) and of the difference wave ( $\Delta f$ ) appear. At  $x = 46$  cm, without the sound signal, the spectrum of a turbulent flow is measured wherein the high frequencies are emphasized. With the sound signal added the spectrum is virtually the same as at  $x = 30$  cm. The boundary layer is stable. The transition point of turbulence is shifted beyond the measuring range of the anemometer probes.

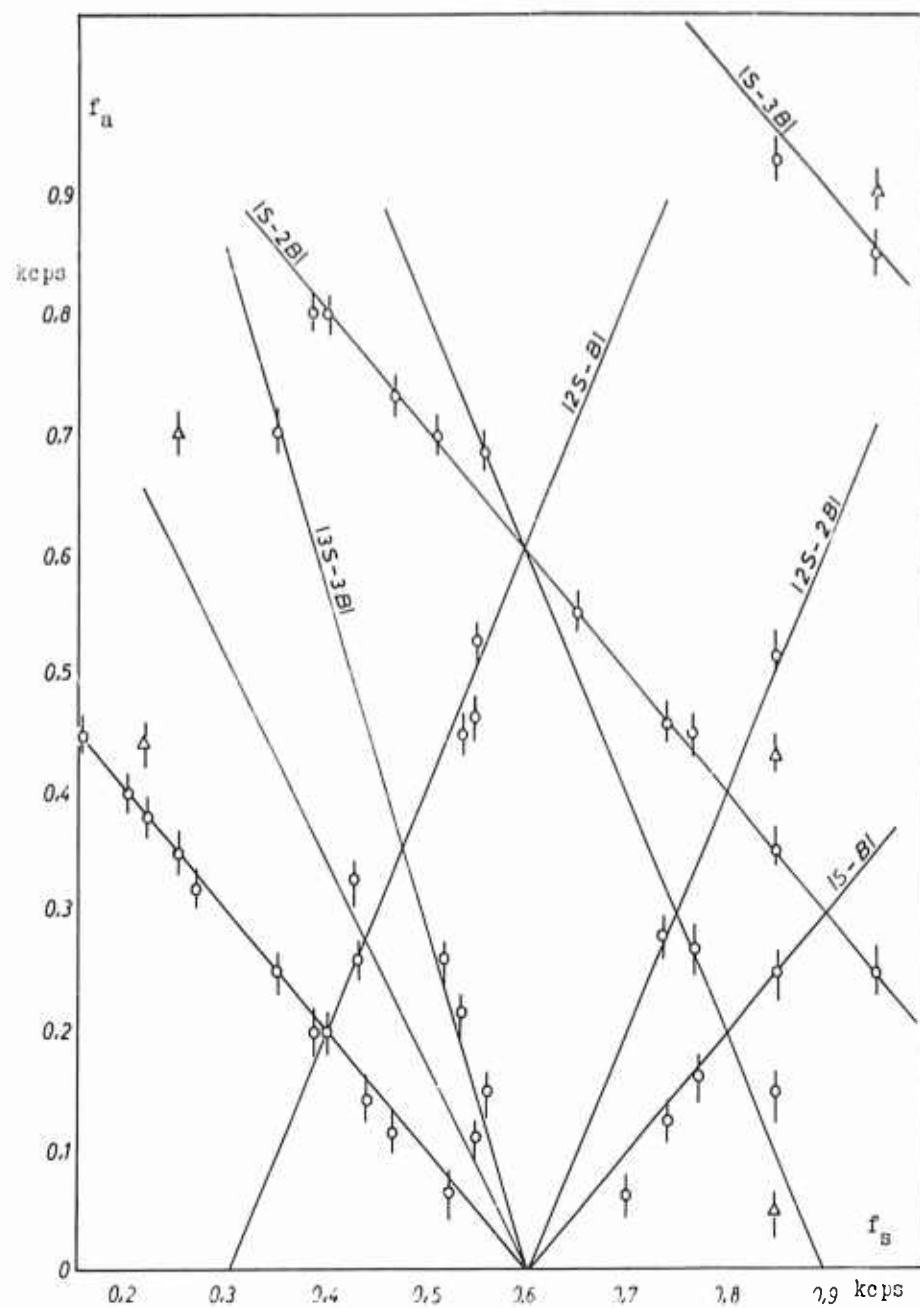


Figure 12 - Distribution of the measured frequencies of boundary layer waves generated by the vibrating ribbon (constant frequency 600 cps) and the variable sound signal with frequency  $f_s$ .

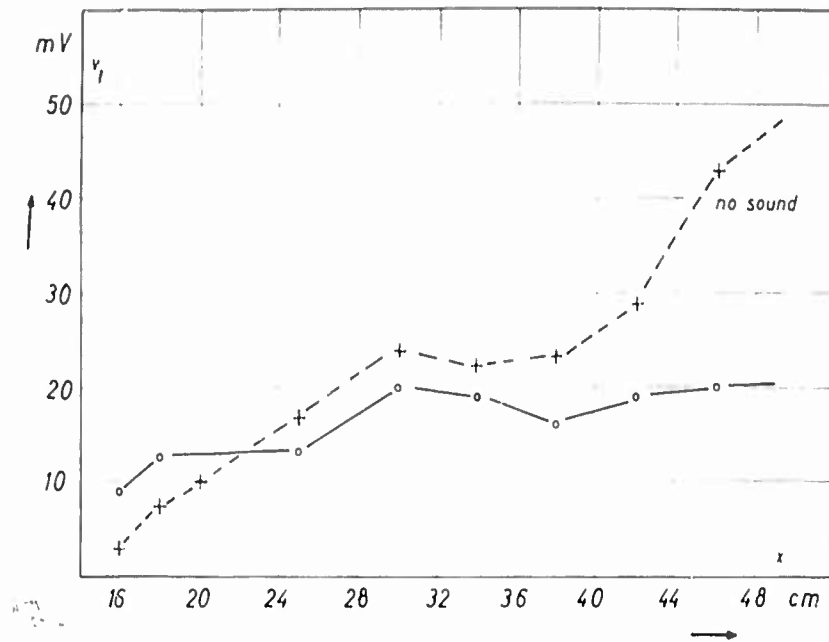


Figure 13 - Suppression of the r. m. s. turbulent velocity oscillations by a sound signal as a function of axial position  $x$ . Frequency of boundary layer wave,  $f_w = 200$  cps. Signal frequency,  $f_s = 300$  cps.

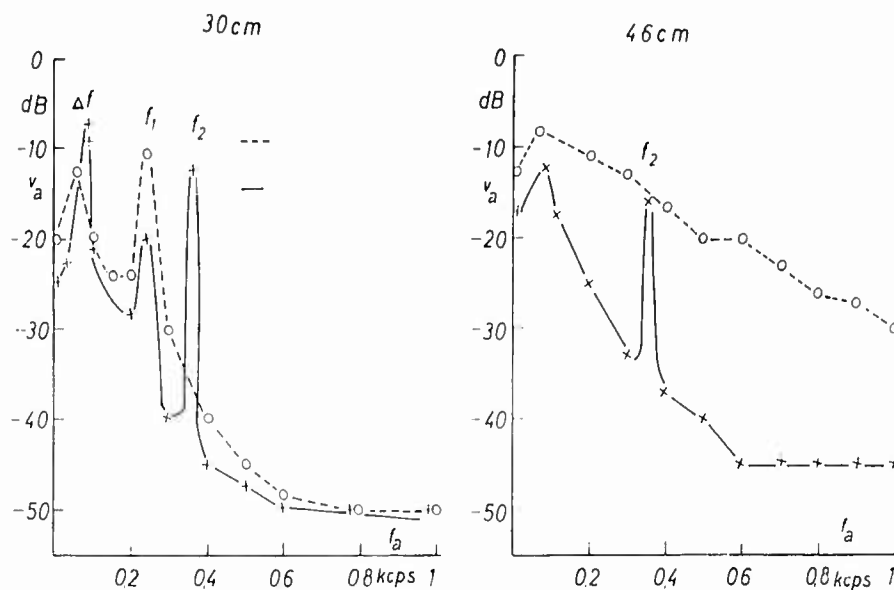


Figure 14 - Spectra of the boundary layer disturbances of Figure 13 with and without sound signal for two positions.

The exact conditions for this stabilization shall be investigated in further measurements. Some measurements indicate that, besides the frequency, the phase relation between the boundary layer wave and the sound signal is also important.

#### IV. Sound Radiated Through a Porous Plate

In a further series of measurements the pistonlike transducer was replaced by a porous plate of sintered bronze. The porous plate was composed of sintered bronze spheres of a diameter of 0.3 to 0.5 mm. The sound signal was generated by a loudspeaker behind the porous plate. It was enclosed in an airtight housing, and therefore, there was no net (i. e., d. c.) air outflow through the plate. The length of the porous plate in the direction of the flow was 10 cm.

For medium amplitudes of the sound signal an excitation of the initial boundary layer disturbances was found similar to those of the pistonlike transducer. This can be seen in Fig. 15 where the distance of the transition point from the leading edge is plotted as a function of the signal frequency. The oscillatory velocity amplitude was held constant at two values indicated by the parameters. The shift of the transition point in the upstream direction indicates a destabilization of the boundary layer. The maximum of the destabilization is in the region between 1 and 2 kcps.

With the anemometer probe at a fixed position and a constant signal frequency, the disturbance level first increases slowly with increasing signal amplitudes. In this amplitude range boundary layer waves of the signal frequency are generated. Then, at a certain frequency-dependent signal level the boundary layer becomes turbulent starting with single turbulent spots. In this amplitude range the disturbance level increases very rapidly with the increasing amplitude. Finally, when the boundary layer is turbulent the distance level is insensitive to a further increase of the signal amplitude.

The sound radiation through a porous plate into the boundary layer can be regarded as a periodic suction and blow-out. In the blow-out phase, air with no velocity component in the flow direction is brought into the boundary layer. This action causes a very strong disturbance to the boundary layer which could explain the lack of suppression of boundary layer disturbances.

At low frequencies the period of the sound signal is large compared to the time of a turbulent spot. In this case for great signal amplitudes the turbulence exciting effect of the signal in the blow-out phase can be directly observed. Fig. 16 shows how the boundary layer becomes turbulent in each blow-out phase. This turbulent eruption is again damped out in the succeeding suction phase.

The object of further measurements will be the combination of a sound signal and a d. c. flow through the porous plate.

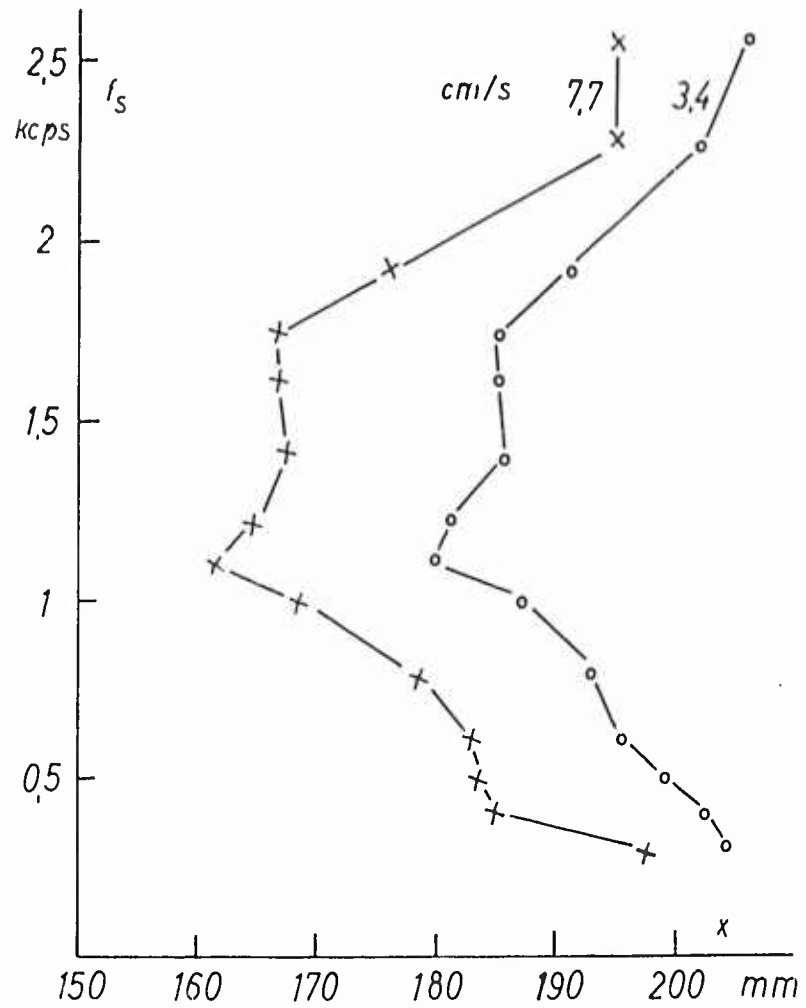


Figure 15 - Shift of the transition point from laminar to turbulent boundary layer by a sound signal through the porous plate.  
Parameter: Signal velocity amplitude above plate.

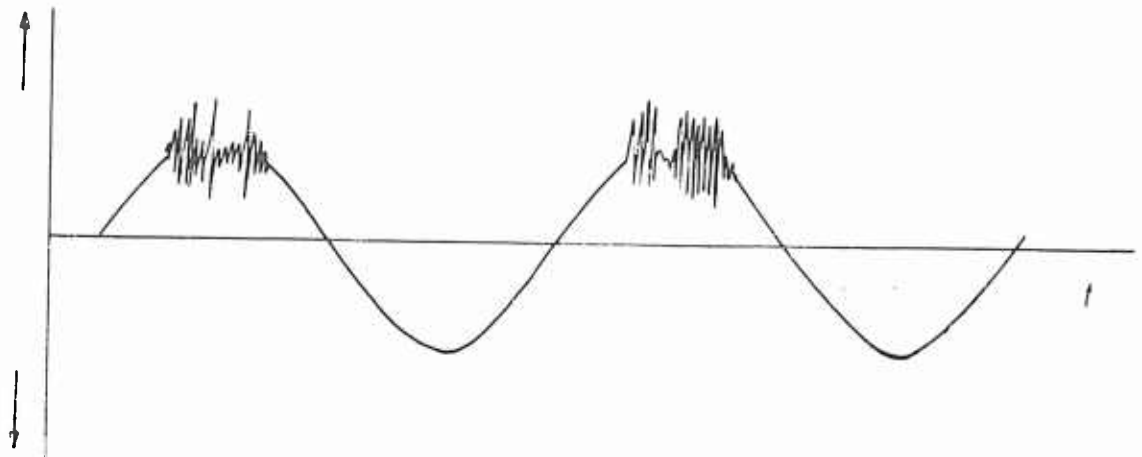


Figure 16 - Turbulent eruptions in the blow-out phases above the porous plate.  
Signal frequency,  $f_s$ , is 200 cps.

## PART B

### SOUND PROPAGATION IN DUCTS WITH SUPERIMPOSED AIR FLOW

The measurements of the cross-distribution of the sound pressure in an absorbing duct showed (ref. 2) at high frequencies an increase of the sound pressure near the absorbing walls. This increase of the sound pressure as compared to that at the center of the duct is caused by the air flow. This effect cannot be explained by a theory which assumes the flow velocity profile in the duct to be flat. It is evident that the pressure increase near the walls is a consequence of the curved flow velocity profile in the real flow.

In the case of a duct with rigid walls and a turbulent flow through the duct an increase of the sound pressure of a downstream propagating signal at the walls of the duct was predicted by a theory by Pridmore-Brown (ref. 4). According to this theory the pressure concentration near the wall is effective only for frequencies for which the acoustic wavelength is of the magnitude of the boundary layer thickness. In a duct with fully developed turbulent flow the boundary layer thickness equals half the free height of the duct.

In the measurements cited above the signal frequencies are below this limit. The mean flow velocities, therefore, change over distances which are smaller than the acoustic wavelength. This statement excludes a solution of the problem by the methods of geometrical acoustics. The object of the present measurements is the influence of a curved flow profile at an absorbing wall on the sound pressure profile and on the propagation constants of the sound wave.

#### I. Experimental Set-up. Rayleigh Absorber -

The experimental set-up in these measurements is virtually the same as in ref. 2. The test section of the duct used so far has a cross-sectional area of  $100 \times 35 \text{ mm}^2$ . Flow velocities up to 200 m/sec are possible. The upper broad side of the test section can be formed by the tested absorber. The acoustic signal is fed into the duct at the inlet into the test section. The sound pressure is registered by a pressure probe which can be moved in the direction of the axis of the duct and normally to the absorber surface. With regard to a high spatial resolution the bore of the pressure probe is 0.5 mm in diameter. Its outer shape is like that of a Pitot tube. The outer tube diameter is 3 mm. The pick-up bore is 9 mm behind the stagnation point of the probe. The output voltage of the microphone connected with the pressure probe is filtered with a bandwidth of 10 cps. The sound pressure at the entrance into the absorbing duct is held constant with the help of a control microphone at that position.

From former measurements it was concluded that the absorber used in these measurements should have constant properties along the duct with a real and frequency-independent input impedance in the examined frequency range. The first requirement is only poorly satisfied by most of the usual porous absorbers. They usually have the further disadvantage of allowing an internal sound propagation parallel to the surface. As a consequence of this fact, the input impedance depends on the shape of the acoustic wave in the duct.

For this reason an absorber was developed which satisfies the above requirements. It consists of layers of corrugated paper and is a type of Rayleigh absorber. The tubes in the corrugated paper which are normal to the absorber surface have a diameter of about 2 mm. The attenuation in these tubes is greater than 20 dB/m for frequencies higher than 1 kcps. With a depth of the absorber of 80 cm the reflections from the rear of the absorber, therefore, can be neglected. For a further reduction of these reflections the tubes are terminated on the rear by a 5 cm layer of rockwool covered by a rigid panel. The whole absorber is enclosed in an air-tight housing which eliminates a net air flow through the absorber and cross-talk into the absorber. At high frequencies a Rayleigh absorber has an asymptotic wall impedance which is determined only by the porosity of the absorber. It is real and independent of frequency. Because of the relatively wide tubes with a flow resistance of about 0.1 rayl the Rayleigh absorber used in these measurements reaches the asymptotic wall impedance at about 1.5 kcps.

In Fig. 17 the real and the imaginary components of the wall impedance of the absorber are plotted vs. frequency. The other graph in Fig. 17 shows the locus diagram of the absorber. The wall impedance is virtually real and constant above 1.5 kcps, its magnitude is  $1.2 \rho c_0$ .

The attenuation in the duct covered with this absorber without flow is plotted in Fig. 18a. Since the wall impedance of the absorber is near the characteristic impedance of air the attenuation is rather high. Because of this high attenuation, in measurements with flow, the signal will disappear in the noise level after a short distance. Therefore, it is reasonable to reduce the attenuation. This is done by a porous foil with the resistance of  $0.25 \rho c_0$  with which the absorber was covered. A further advantage of this foil is a smoother surface for the absorber. The attenuation without flow for this absorber is plotted in Fig. 18b.

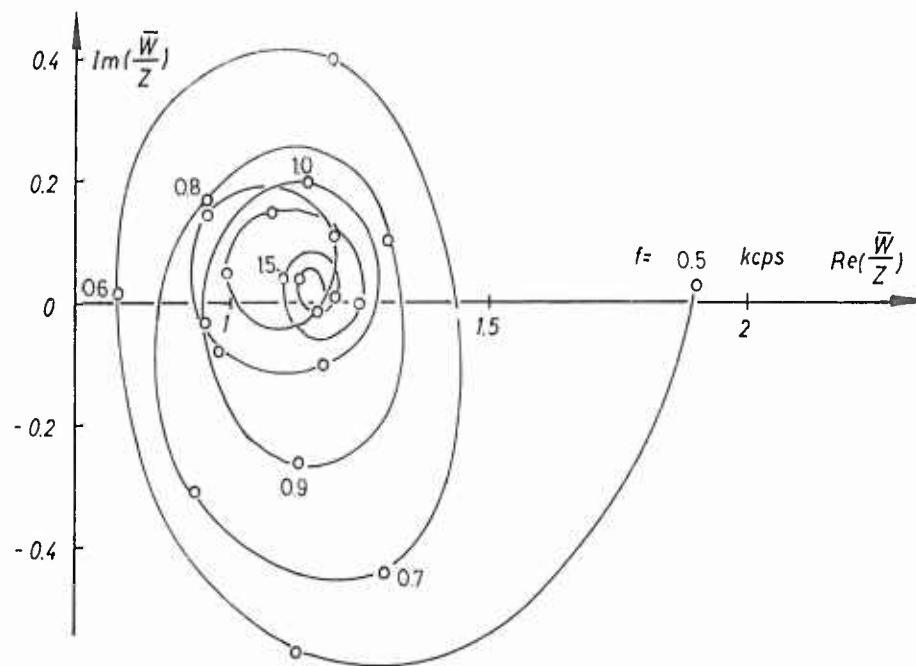
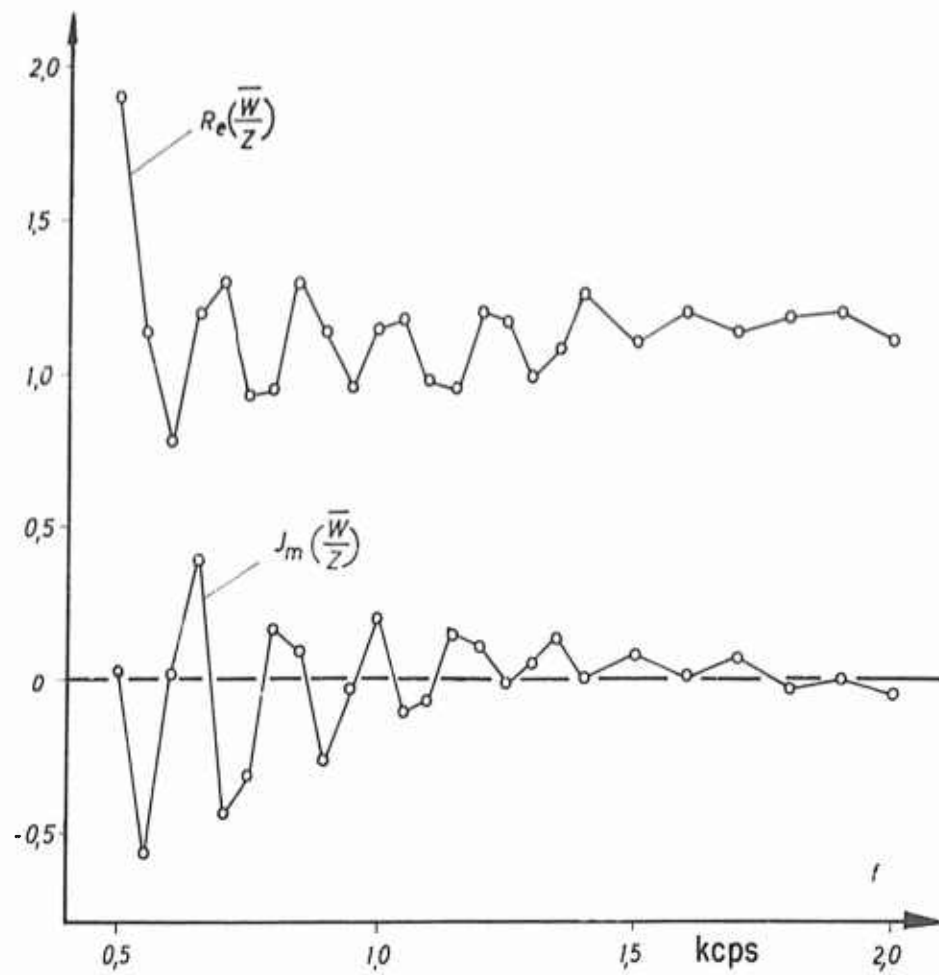


Figure 17 - Wall impedance of a Rayleigh absorber with finite thickness.



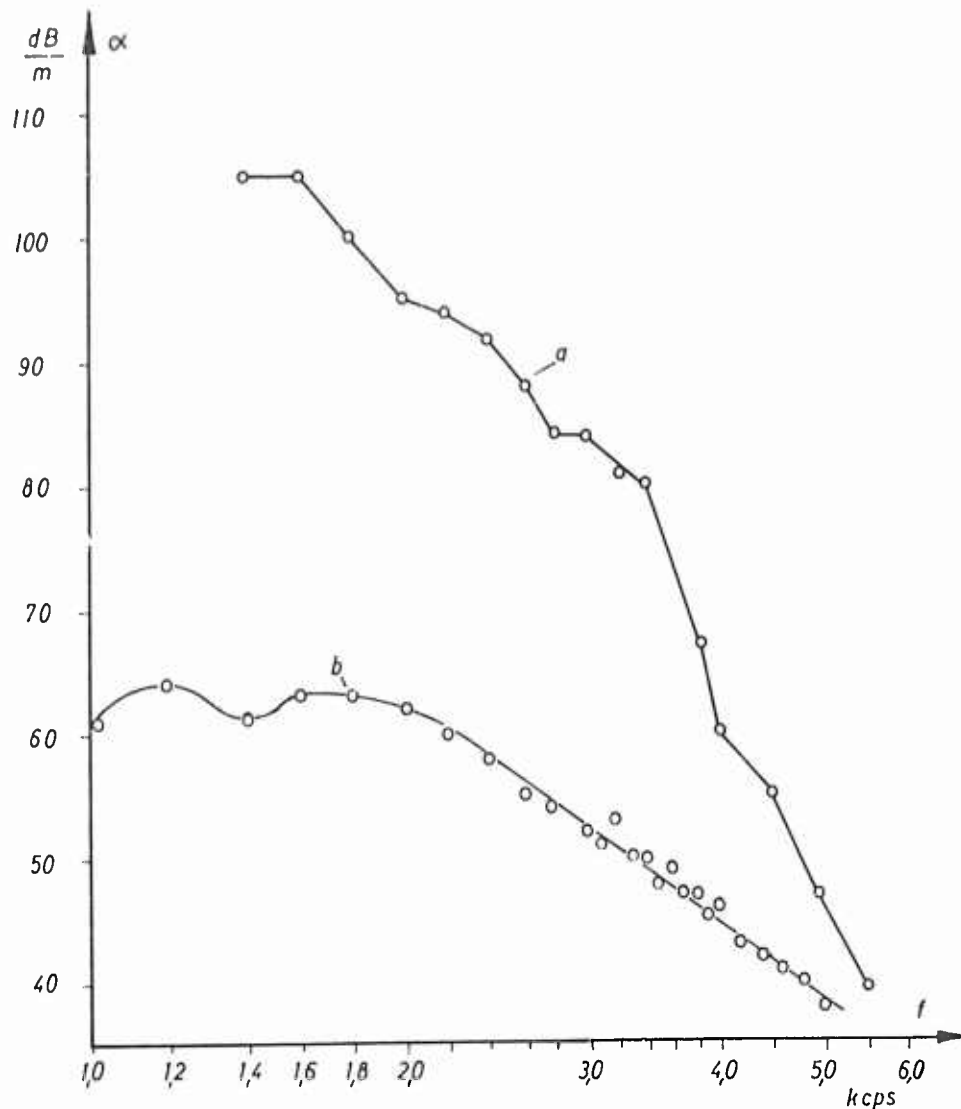


Figure 18 - Attenuation in the duct coated with (a) the Rayleigh absorber, and (b) a Rayleigh absorber covered with a porous foil.

## II. Sound Pressure Profiles -

The sound pressure profiles are measured at high frequencies. Above 3.4 kcps strong fluctuations of the sound pressure along the axis of the duct (10 cm wide) was measured. It is maximum in the duct with rigid walls (20 dB). In the absorbing section of the duct these sound pressure fluctuations decrease together with the sound level. This effect, decreasing the fluctuations, is lessened as the frequency is increased. At 3.4 kcps the width of the duct equals one wavelength. The fluctuation indicates the existence of higher modes which could not be eliminated by symmetric excitation of the signal. Due to the fluctuation the shape of the sound pressure profile depends strongly on the measuring position.

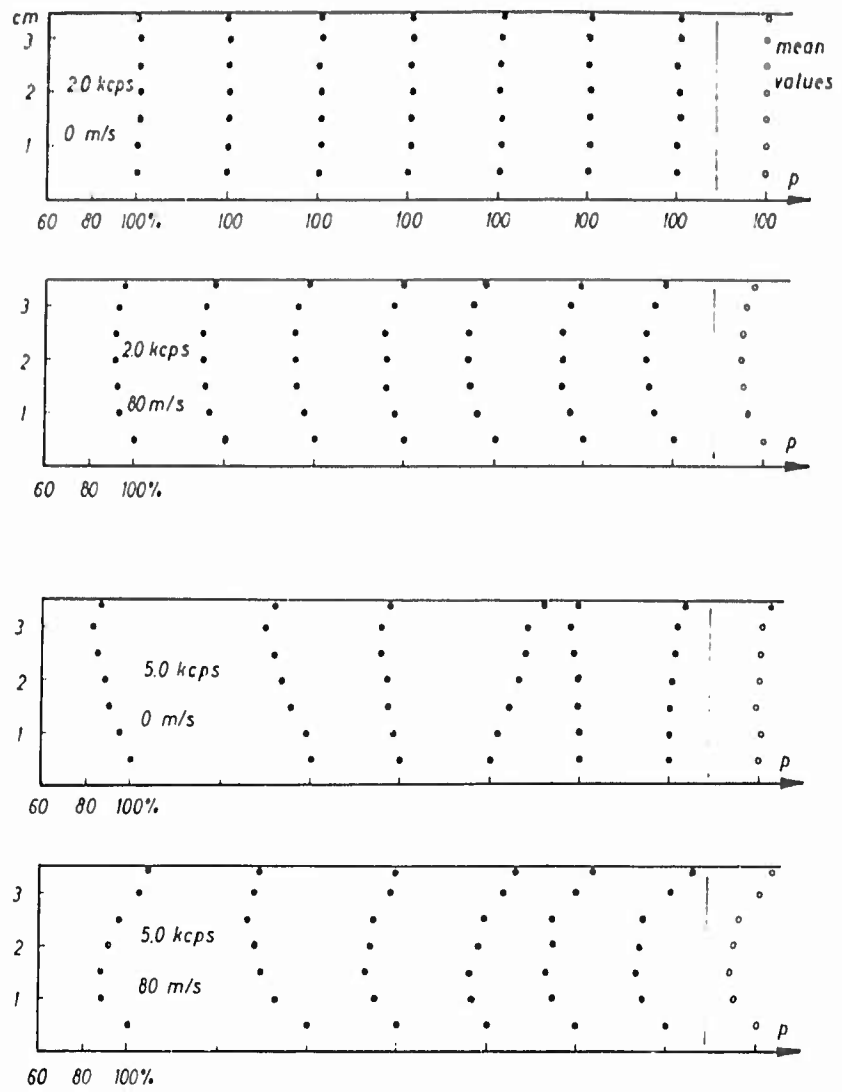
For the measurements reported below, therefore, the width of the duct was reduced to 6.5 cm. The limiting frequency then is about 5.5 kcps. The fluctuation could be reduced to 2 dB in the maximum. The remaining fluctuations in the pressure amplitude distribution along the duct must be ascribed to inhomogeneities.

The accuracy of the measurement was improved by averaging several sound pressure profiles which were measured in a section 24 cm long. The measuring positions were 4 cm distant from one another.

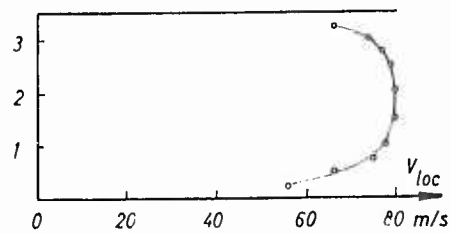
In Fig. 19 these individual sound pressure profiles are shown for a duct with rigid walls and a flow velocity of 80 m/sec. Sound propagation and flow are in the same direction. Sound pressure measurements are normalized on a percentage basis to the 0.5 cm position, the relative 100 percent position. The distance from the bottom is the ordinate. The scale of the axes in all figures is the same as that indicated in the first figure. The value of 100 percent on the abscissa is indicated for each graph. The profile on the right side of each row is the averaged one. In these graphs the deviation of the individual profiles from the averaged one are small for the frequency 2.0 kcps. For 5.0 kcps however (i. e. near the limiting frequency) the deviations are rather great.

In Fig. 20 are plotted the averaged sound pressure profiles in the rigid duct for several frequencies and the two flow velocities 0 and 80 m/sec. As it was expected, the sound pressure profiles are flat for zero flow velocity. With the superimposed flow, however, the sound pressure is increased near the walls of the duct. This rise increases with increasing frequency. A flow with a flat velocity profile would result in a flat sound pressure profile (ref. 2). The curvature of the sound pressure profiles, therefore, is caused by the gradient of the mean flow velocity. The flow velocity profile is plotted in Fig. 19, too. The small asymmetry in the sound pressure profiles of Fig. 19 seem to be caused by corresponding asymmetries in the mean flow velocity profiles.

In Fig. 21 corresponding sound pressure profiles are plotted for the absorbing duct. The section in which the averaged profiles are measured begins at 5 cm behind the entrance into the absorbing duct. In Fig. 21 again individual and averaged profiles are shown. At the low frequency of 2.0 kcps the deviations from the averaged profile again are small. This indicates that a stationary sound pressure profile is formed between the entrance into the absorbing duct and the measuring position. As with the rigid walls the deviations of the profiles at 5.0 kcps are greater. The averaged profiles for zero and 80 m/sec flow velocities are represented in Fig. 22. Without flow the profiles reflect the usual fact of decreasing sound pressure near the absorber. All profiles reveal a small convex curvature. With superimposed flow, however, the sound pressure profiles become concave. This again is the influence of the flow velocity gradient.



(a) Sound Pressure Distribution



(b) Flow Velocity Profile at  $V = 80$  m/sec

Figure 19 - Sound pressure and flow velocity profiles for a duct with rigid walls.

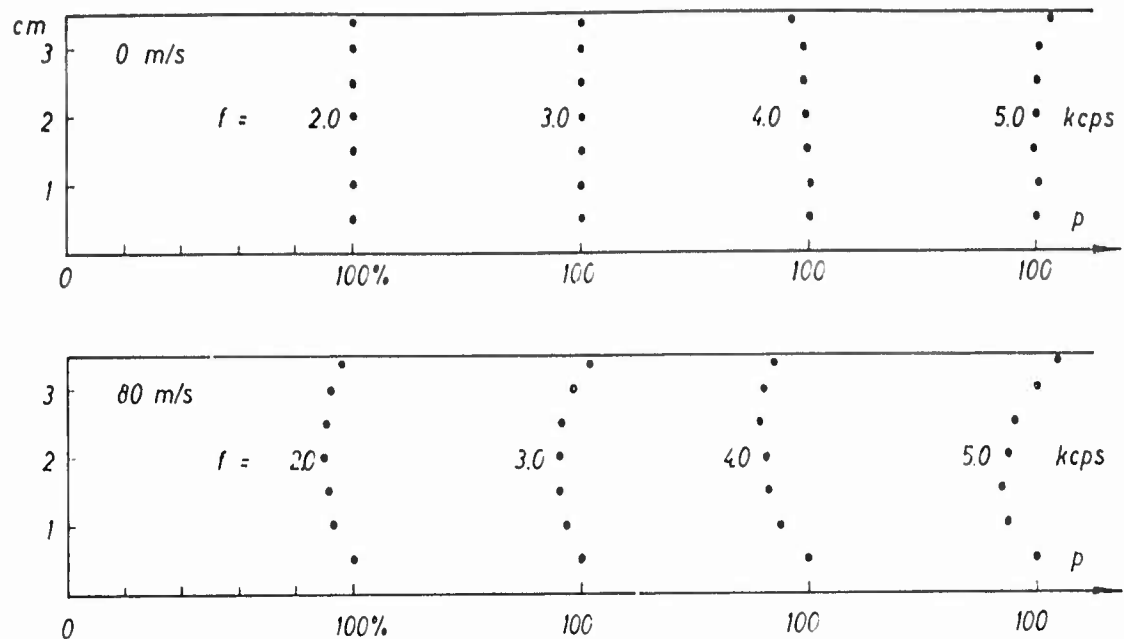


Figure 20 - Sound pressure distribution in the duct with rigid walls at  $V = 0$  and  $V = 80$  m/sec. Averaged profiles.

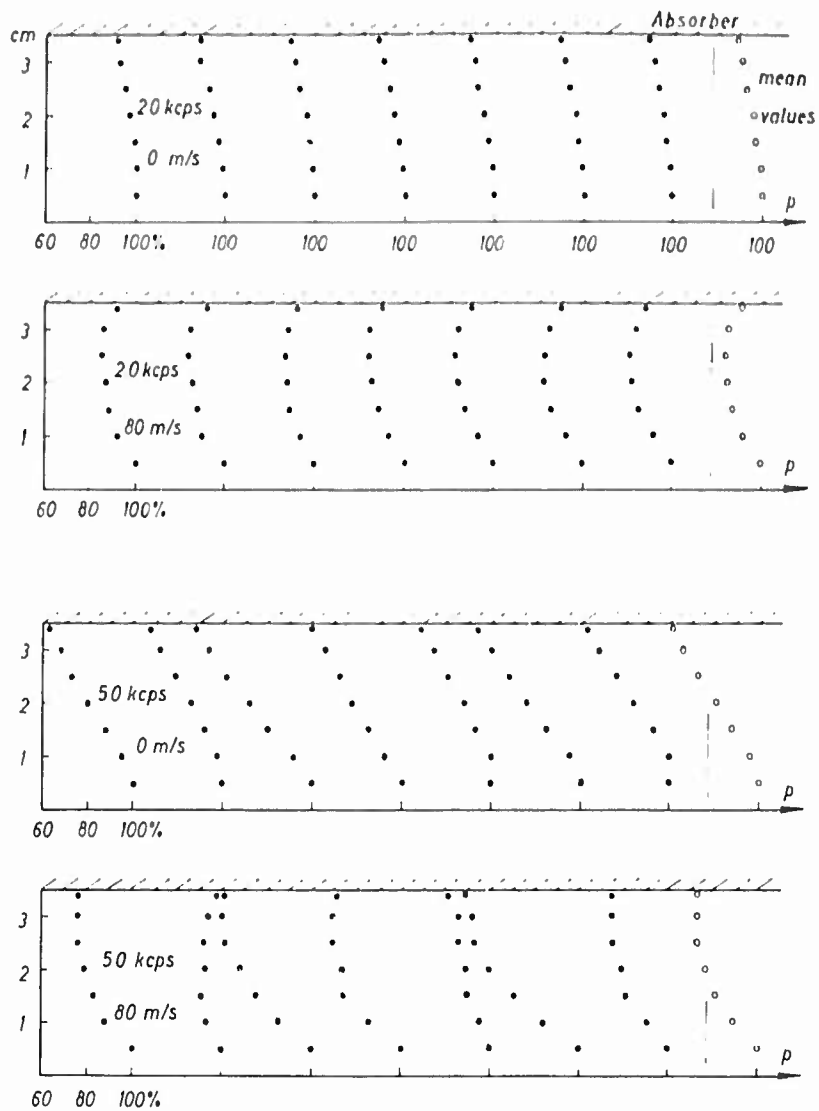
The superposition of flow with a flat velocity profile would change the lateral wavenumber of the sound wave in the absorbing duct (ref. 2). This effect too would change the sound pressure profile. In order to eliminate this kind of profile variation the measured sound pressure profiles have to be compared with the profiles without flow at equivalent frequencies  $f_{eq}$ . This equivalent frequency is chosen to have the same sound wavelength in the duct as the measuring frequency with superimposed flow. For this elimination the absorber has to be frequency-independent. In Fig. 22 the equivalent profiles measured at zero flow velocity are added for comparison. The pressure amplitudes were normalized to equal sound pressure in front of the absorber.

### III. Attenuation -

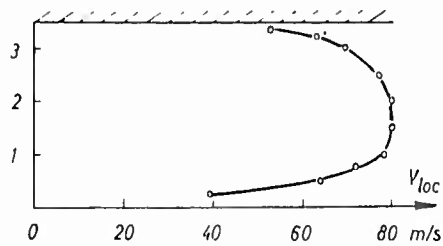
The attenuation constant in a duct with an absorber with real wall impedance is equal to the ratio of the acoustic power per unit length penetrating into the absorber to the acoustic energy flux through the duct,

$$W = \int_0^h I(z) dz$$

$h$  = height of the duct,  $I(z)$  = acoustic intensity,  $W$  = power flux. Since the input impedance of the absorber is real, the absorbed energy per unit length is proportional to the square of the sound pressure at the absorber surface.



(a) Sound Pressure Distribution



(b) Flow Velocity Profile at  $V = 80$  m/sec

Figure 21 - Sound pressure and flow velocity profiles in the sound absorbing duct.

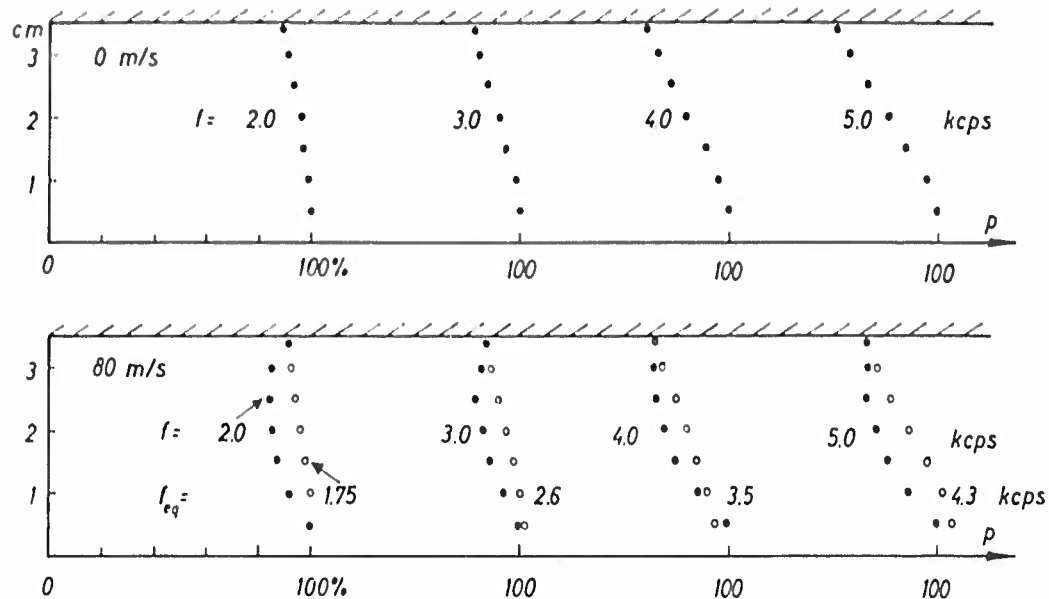


Figure 22 - Sound pressure distribution in the sound absorbing duct at  $V = 0$  and  $V = 80$  m/sec. Averaged profiles.

In Fig. 22 the sound pressures at the absorber are equal for both the measuring frequency and the equivalent frequency. The energy flux  $W$ , however, under these conditions is smaller with superimposed air flow than it is without flow. For an air flow with a curved velocity profile the sound attenuation, therefore, is greater than it is with a flow having a flat velocity profile. By numerical integration of the measured sound pressure profiles for the energy flux  $W$  an increase of the sound attenuation, approximately 15 percent, is obtained due to the curved flow velocity profile. From the limited amount of data taken to date, indications are that the additional sound attenuation is directly proportional to the sound signal frequency.

#### IV. Conclusions -

The measurements reported above indicate that the attenuation of a sound wave propagating in a downstream direction is greater for a curved velocity profile than for a flat velocity profile. The acoustic energy is refracted towards the absorber by the gradient of the flow velocity. The refraction is considerable, even for wavelengths (7 to 15 cm) greater than the boundary layer thickness (1.8 cm).

As already mentioned the sound propagation in absorbing ducts has been described by a theory in which the flow velocity profile was assumed to be flat (ref 2). The comparison of that theory with the experimental results obtained for a porous absorber revealed rather good agreement as long as

the input impedance of the absorber was real. In the medium frequency range where the impedance of the absorber used had a reactive component, the attenuation predicted by the theory was greater than the experimental value. From the measurements reported above it follows that this difference would become even greater if the theory would take into account the curvature of the flow velocity profile. In search for the cause of this difference the only explanation can be that the input impedance of the absorber is changed by the turbulent flow. The more reactive the absorber impedance is the more the sound attenuation is affected by the change of the impedance due to the flow. The investigation of this behavior shall be the object of future work. A part of these investigations will be the completion of the theory of sound propagation in absorbing ducts with respect to an air flow with a curved flow velocity profile.

## PART C

### INFLUENCE OF FLOW THROUGH AN ORIFICE ON ITS RADIATION IMPEDANCE

In a tube with a flow discharge at its orifice a plane sound wave propagating in the downstream direction is added to the flow. The sound wave is partially reflected at the orifice and a standing wave in the tube is set up. From this point the reflection factor  $\underline{r} = r \cdot e^{j\psi}$  and the radiation impedance of the orifice are evaluated. (Underlined symbols are complex.) The object of the following measurements is to investigate the influence of the flow discharge and of the turbulent flow field behind the orifice on its radiation impedance.

#### I. Experimental Set-up -

The air flow is generated by a centrifugal blower and silenced by a subsequent silencer (ref. 3). Behind the silencer the flow turbulence is reduced by gauze screens, smoothing pipes and the contraction cone in front of the measuring tube (contraction ratio 1:24). The contour of the contraction cone is shaped after a polynomial of 9th degree which was chosen to reduce the turbulence to a minimum (ref. 3).

The measuring tube is a circular brass tube of 85 mm inner diameter (2 meters long, wall thickness 5 mm). The sound signal is fed into the tube at its upstream end from one or two pressure chamber loudspeakers (200 watts each).

The sound pressure in the tube is picked up by a microphone probe. The probe is on the axis of the tube and is inserted through the discharge orifice of the tube. The influence of the probe tube on the sound field can be neglected (ref 1) because its cross-sectional area is smaller than 1 percent of the area of the flow tube. The net dynamic-range of the microphone is limited by the cross-talk through the walls of the probe tube. It is greater than 50 dB for frequencies between 1 and 2 kcps, at lower frequencies it is greater than 65 dB. The frequency range of the set-up is limited towards low frequencies by the length of the tube (lower limit about 250 cps) and towards high frequencies by the onset of the higher modes. This upper frequency limit will be at  $k \cdot a = 1.84$  ( $2a = \text{tube diameter}$ ), that is at 2.36 kcps. The output voltage of the microphone is filtered with a bandwidth of 10 cps.

The flow velocity is measured by a Pitot tube on the axis of the measuring tube at a distance of 80 cm from the discharge orifice. The maximum available flow velocity is about 180 m/sec. The temperature of the air is held constant by a cooler. The sound velocity in the tube without flow is 341.5 m/sec.



## II. Impedance Formula -

The radiation impedance and the reflection factor of the discharge orifice are evaluated from the measured standing wave ratio, the distance of the first pressure minimum from the orifice and the distance between adjacent minima.

The phase velocities of the sound wave in the tube for the two propagation directions can be written:

$$c_v = c_o \pm V$$

where  $V$  is an appropriate flow velocity. The propagation exponents are:

$$\text{without flow:} \quad k_o = \beta_o - j\alpha_o ,$$

$$\text{for downstream propagation:} \quad k_1 = k_o / (1 + M), \quad M = V/c_o$$

$$\text{for upstream propagation:} \quad k_2 = k_o / (1 - M),$$

where  $\beta$  is the phase constant and  $\alpha$  is the attenuation constant. From former measurements it is known that in a rigid duct the attenuation per wavelength is virtually constant:

$$\alpha_o \lambda_o = \alpha_1 \lambda_1 = \alpha_2 \lambda_2 .$$

The sound pressure in the tube is represented by

$$\underline{p} = \underline{p}_o \left[ e^{-jk_1 x} + r \cdot e^{j(k_2 x + \psi)} \right] .$$

The reflection factor  $\underline{r} = r \cdot e^{j\psi}$  shall be determined.

The conditions for the maximum and the minimum of the sound pressure in the standing wave respectively are:

$$\text{maximum:} \quad \cos \left[ 2\beta_o x / (1 - M^2) + \psi \right] = 1$$

$$\text{minimum:} \quad \cos \left[ 2\beta_o x / (1 - M^2) + \psi \right] = -1.$$

From this, standing wave ratio is

$$d = \frac{P_{\min}}{P_{\max}} = \frac{1 - re^{2\alpha x}}{1 + re^{2\alpha x}}$$

$$\alpha = \frac{a_0}{1 - M^2} .$$

The standing wave ratio as a function of  $x$  is extrapolated to  $x = 0$  and the magnitude of the reflection factor is determined from

$$d_{x=0} = \frac{1 - r}{1 + r} .$$

From the above condition for the sound pressure minima the distance  $\Delta x$  between two adjacent minima is

$$\Delta x = (1 - M^2) \frac{\lambda_0}{2} . \quad (1)$$

From the condition of the position at  $x = -s$ ,  $s > 0$ , of the first minimum nearest to the tube orifice the phase angle of the reflection factor becomes

$$\psi = \pi \frac{s - \Delta x/2}{\Delta x/2} . \quad (2)$$

From the reflection factor of the orifice its impedance  $\underline{W}$  will be determined. The influence of the attenuation in the tube on the standing wave will be neglected in the following equations.

Without flow the impedance of the orifice is calculated from

$$\underline{W} = Z_0 \frac{1 + re^{j\psi}}{1 - re^{j\psi}} , \quad Z_0 = \rho c_0 . \quad (3)$$

In a tube with rigid walls and constant flow velocity  $V$ , Newtons equation

$$\frac{d\bar{v}}{dt} = - \text{grad } p \quad , \quad \bar{v} = v + V \quad , \quad v = \text{oscillatory velocity}$$

the equation of continuity

$$\text{div} (\rho \bar{v}) = - \frac{\partial \rho}{\partial t}$$

and the adiabatic equation

$$dp = c_0^2 d\rho$$

are combined to the linearized equations

$$\rho \frac{\partial v}{\partial t} = - \rho V \frac{\partial v}{\partial x} - \frac{\partial p}{\partial x} \quad (4)$$

and

$$\rho \frac{\partial v}{\partial x} = - \frac{V}{c_0^2} \frac{\partial p}{\partial x} - \frac{1}{c_0^2} \frac{\partial p}{\partial t} \quad (5)$$

They are combined to the wave equation

$$\frac{\partial^2 p}{\partial t^2} = c_1^2 c_2^2 \frac{\partial^2 p}{\partial x^2} - 2V \frac{\partial^2 p}{\partial t \partial x} \quad (6)$$

with the solution

$$p(t, x) = p_0 \left[ e^{-jk_1 x} + r e^{j(k_2 x + \psi)} \right] e^{j\omega t} \quad (7)$$

where

$$c_1 = c_o + V, \quad c_2 = c_o - V, \quad k_1 = \frac{\omega}{c_1}, \quad k_2 = \frac{\omega}{c_2}.$$

The relation between the oscillatory sound velocity  $v$  and the sound pressure  $p$  follows from Eq 4 and Eq 5:

$$\rho \frac{\partial v}{\partial t} = \frac{M}{c_o} \frac{\partial p}{\partial t} - (1 - M^2) \frac{\partial p}{\partial x}. \quad (8)$$

Insertion of Eq 7 into Eq 8 results in

$$v = \frac{p_o}{Z_o} \left[ e^{-jk_1 x} - r e^{j(k_2 x + \psi)} \right]. \quad (9)$$

Finally, from Eq 9 and Eq 7, the relation between the impedance of the orifice at  $x = 0$  and its reflection factor is

$$\frac{W}{v} = \left( \frac{p}{v} \right)_{x=0} = Z_o \frac{1 + r e^{j\psi}}{1 - r e^{j\psi}}. \quad (10)$$

This is the same equation as without flow.

### III. Preliminary Measurements -

#### III.1. Flow Velocity -

In the above equation a flow velocity  $V$  was defined by

$$c_{1,2} = c_o \pm V.$$

The flow velocity profile in the tube is curved. The measured flow velocity  $V'$  is the axial flow velocity near the discharge orifice where the velocity profile is stationary. For the evaluation of the reflection factor the flow velocity  $V$  was computed from Eq 1 for the distance between adjacent sound pressure minima. The measurements yielded the relation

$$V = 0.85 V' \quad (11)$$

between the two velocities independent of frequency and flow velocity. From the general equation of the flow velocity profile of a turbulent flow in a cylindrical tube at the Reynolds number  $10^6$  which is typical for the present measurements the relation between the averaged flow velocity  $V_{av}$  in the tube and the maximum flow velocity  $V'$  on the axis of the tube is (ref. <sup>av</sup>6)

$$V_{av} = 0.84 V' .$$

From this it can be concluded that the sound wave is convected by the flow with the average flow velocity,  $V = V_{av}$ .

A further indication of this fact comes from the following measurements: In the standing wave within the tube all distances between adjacent sound pressure minima were measured for the axial flow velocities  $V' = 80, 120$  and  $160$  m/sec. The velocity  $V$  evaluated from Eq 1 proved to be constant within the accuracy of the measurement (smaller than 1 percent).

### III. 2. Radiation Impedance

The influence of several parameters on the radiation impedance of the orifice were investigated. The accuracy of the measurements, therefore, were as good as possible. The measurements of  $r$  without flow agreed with the theoretical values of  $r$  within 3 percent (see Figure 23). The inaccuracy of the phase measurements increases with  $ka$ , i. e. with decreasing wavelength. It is

for  $ka = 0.8$  about 2.5 percent  
and for  $ka = 1.6$  about 6 percent. (Figure 24)

For the evaluation of the influence of the sound field in the room surrounding the discharge orifice the measurements without flow were repeated in the anechoic chamber. There was, however, no improvement of the measuring accuracy.

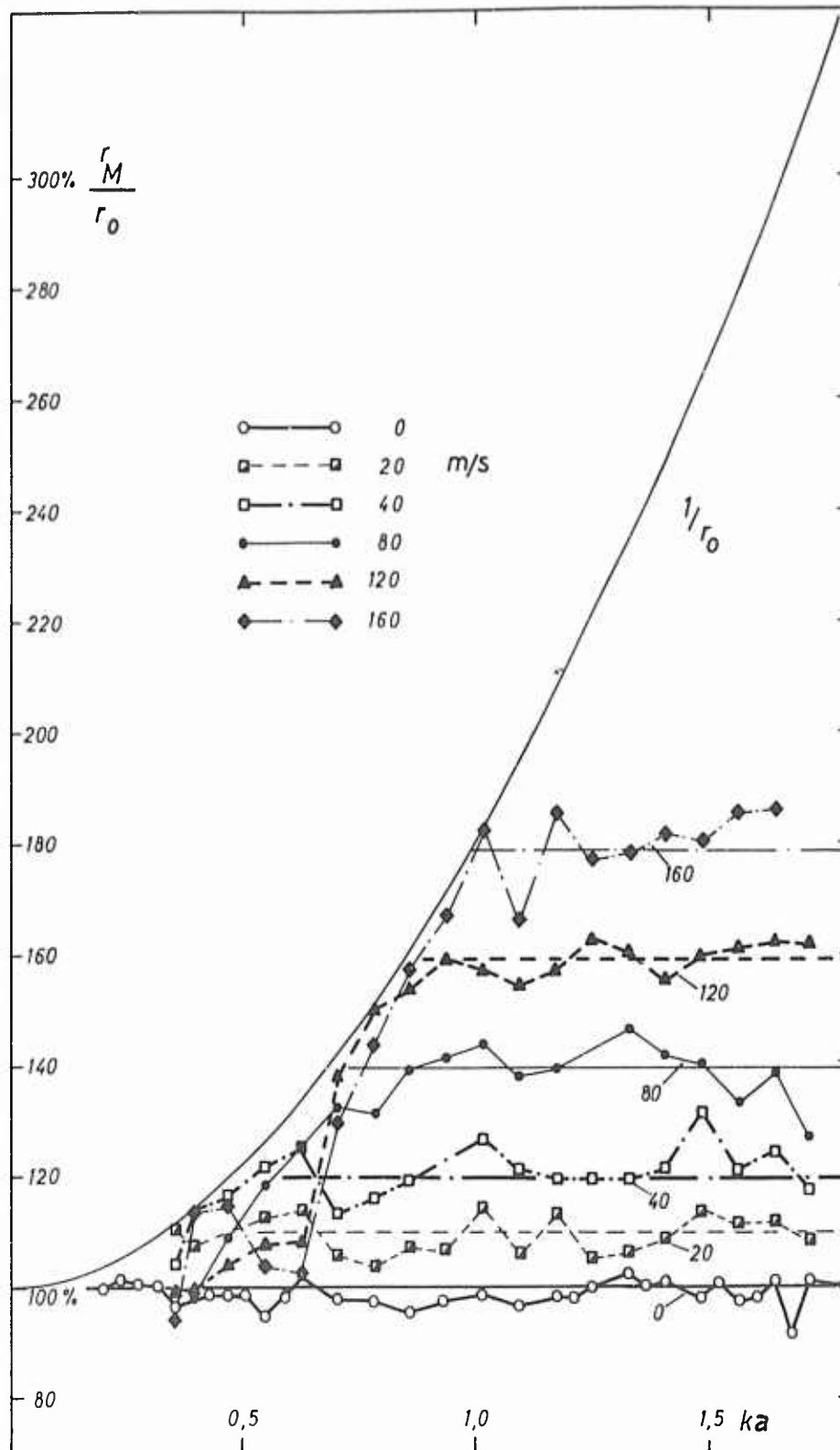


Figure 23 - Reflection factors  $r_M$  of the orifice in a baffle normalized with the theoretical value  $r_0$  without flow vs.  $ka$ . Parameter: Axial flow velocity  $V'$ .

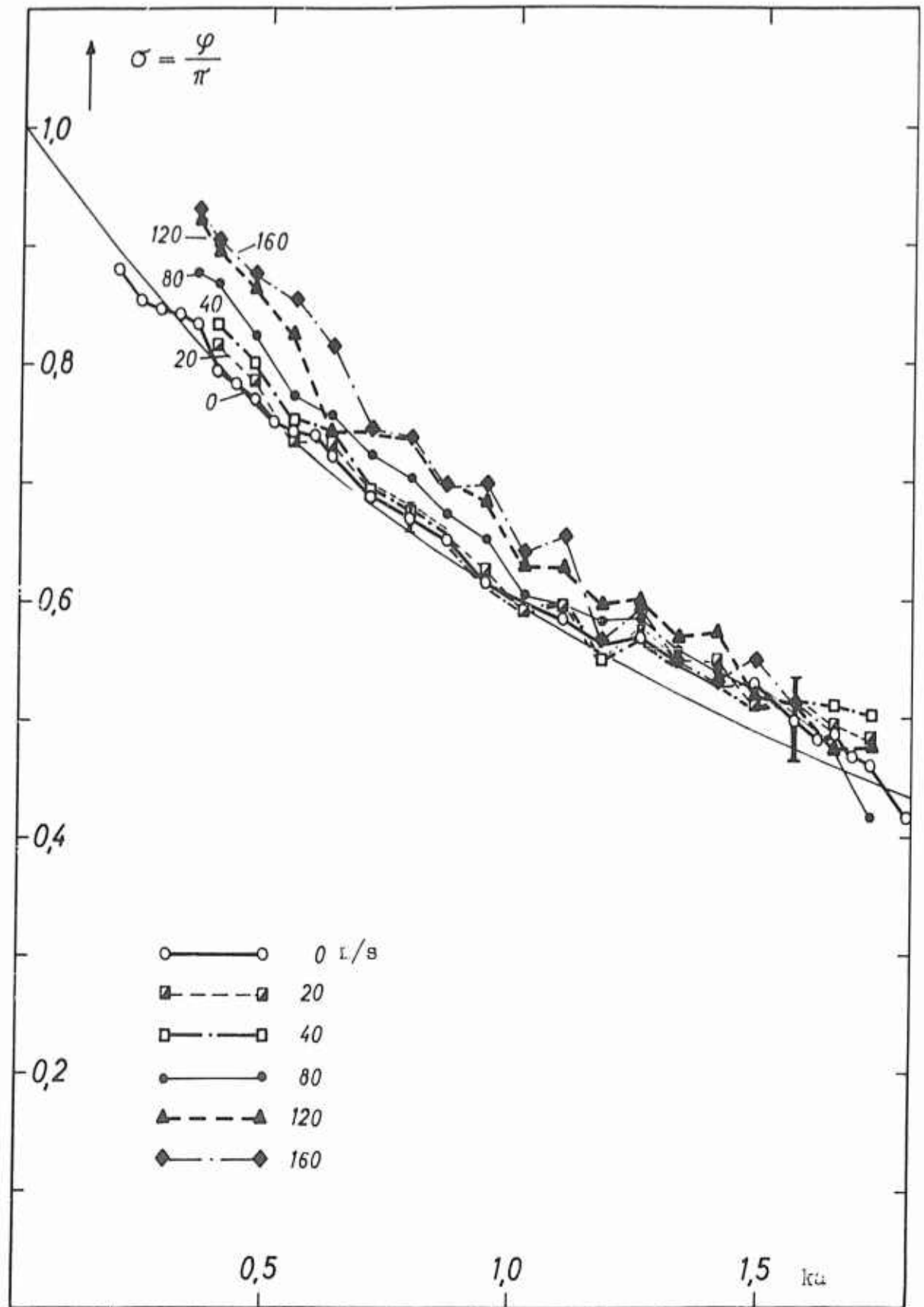


Figure 24 - Normalized phase angle  $\sigma = \psi / \pi$  of the reflection factor of the orifice in a baffle vs.  $ka$ . Parameter: Axial flow velocity  $V'$ .

#### IV. Impedance Measurements -

##### IV.1. Unflanged Orifice and Orifice in a Baffle -

The impedance of the tube orifice was measured in the velocity range between 0 and 160 m/sec. Measurements completed to date are the impedance of the unflanged orifice and the impedance of the orifice in a baffle of  $1.85 \times 2 \text{ m}^2$ .

The real and imaginary components of the impedance

$$\underline{W} = R + jX$$

are plotted in Figure 25 and Figure 26 in a normalized representation as functions of  $ka$ :

$$ka = \frac{2\pi f}{c_0} \cdot a$$

$f$  = frequency,  $a$  = inner radius of tube,  $c_0$  = sound velocity without flow ( $c_0 = 341.5 \text{ m/sec}$ ).

For higher  $ka$ -values the influence of the flow is reflected in a parallel shift of the curves towards smaller  $R/\rho c_0$  values, as shown in Figure 27. For smaller  $ka$ -values the measuring accuracy becomes smaller because here the standing wave ratio  $d = p_{\min}/p_{\max}$  increases with increasing distance from the discharge orifice, in contrast to the theory.

In Figure 24 the phase angle  $\psi$  of the reflection factor is represented in the form  $\sigma = \psi/\pi$ . The phase angle is unaffected by the measuring inaccuracy in the determination of  $r$  for small values of  $ka$ . The phase angle is virtually constant for all flow velocities. Only for small values of  $ka$  is there a small increase of  $\psi$  with the flow velocity. The scattering of the measurements at higher  $ka$ -values is within the amount of the inaccuracy of the measurement.

The imaginary component of the impedance decreases with increasing flow velocity for small values of  $ka$ , at greater  $ka$  values it increases with the flow velocity. The change of the imaginary component for small  $ka$  is mainly a consequence of the change of  $\psi$  whereas for great  $ka$  the change of  $r$  becomes important.



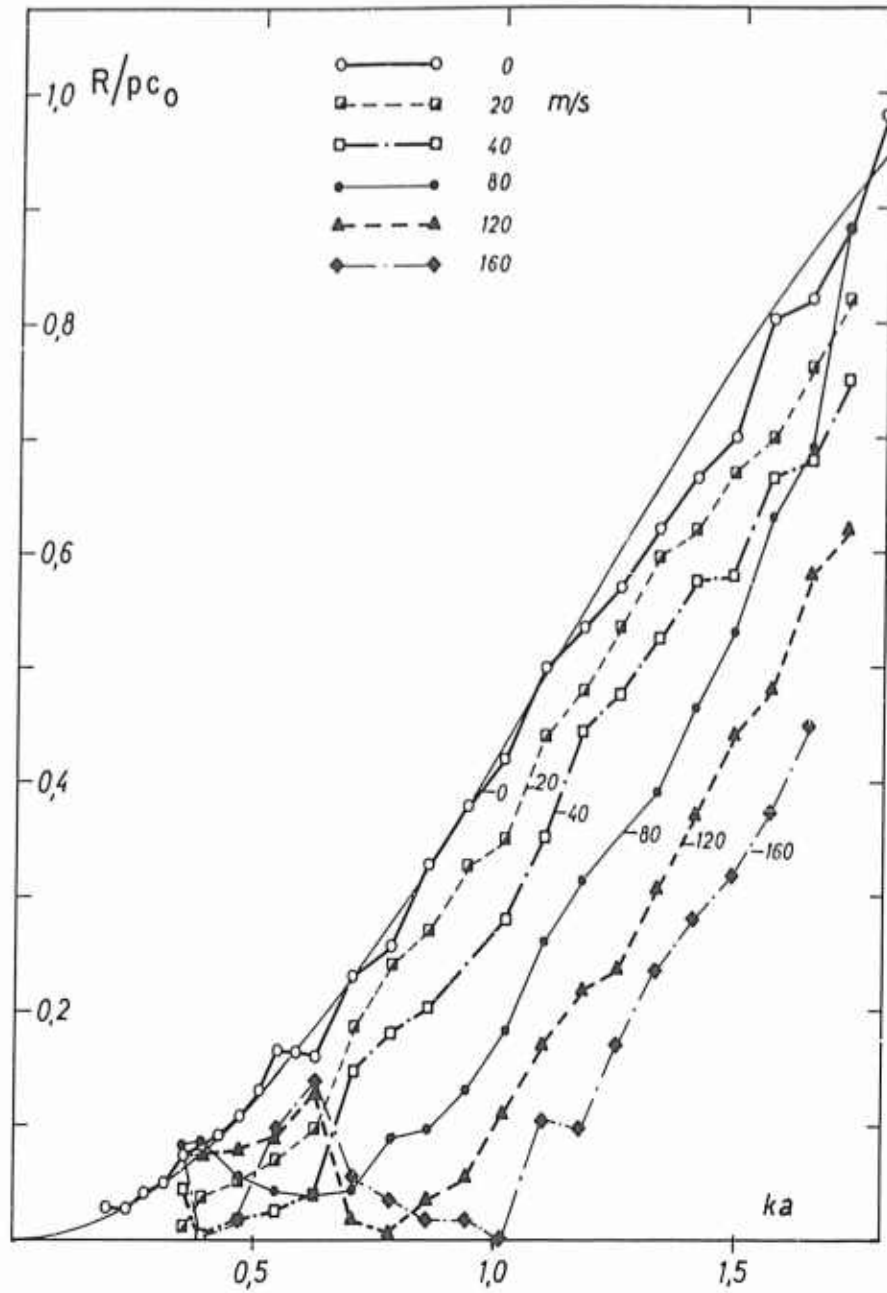


Figure 25 - Normalized real part  $R/\rho c_0$  of the radiation impedance of the orifice in a baffle vs.  $ka$ . Parameter: Axial flow velocity  $V'$ .

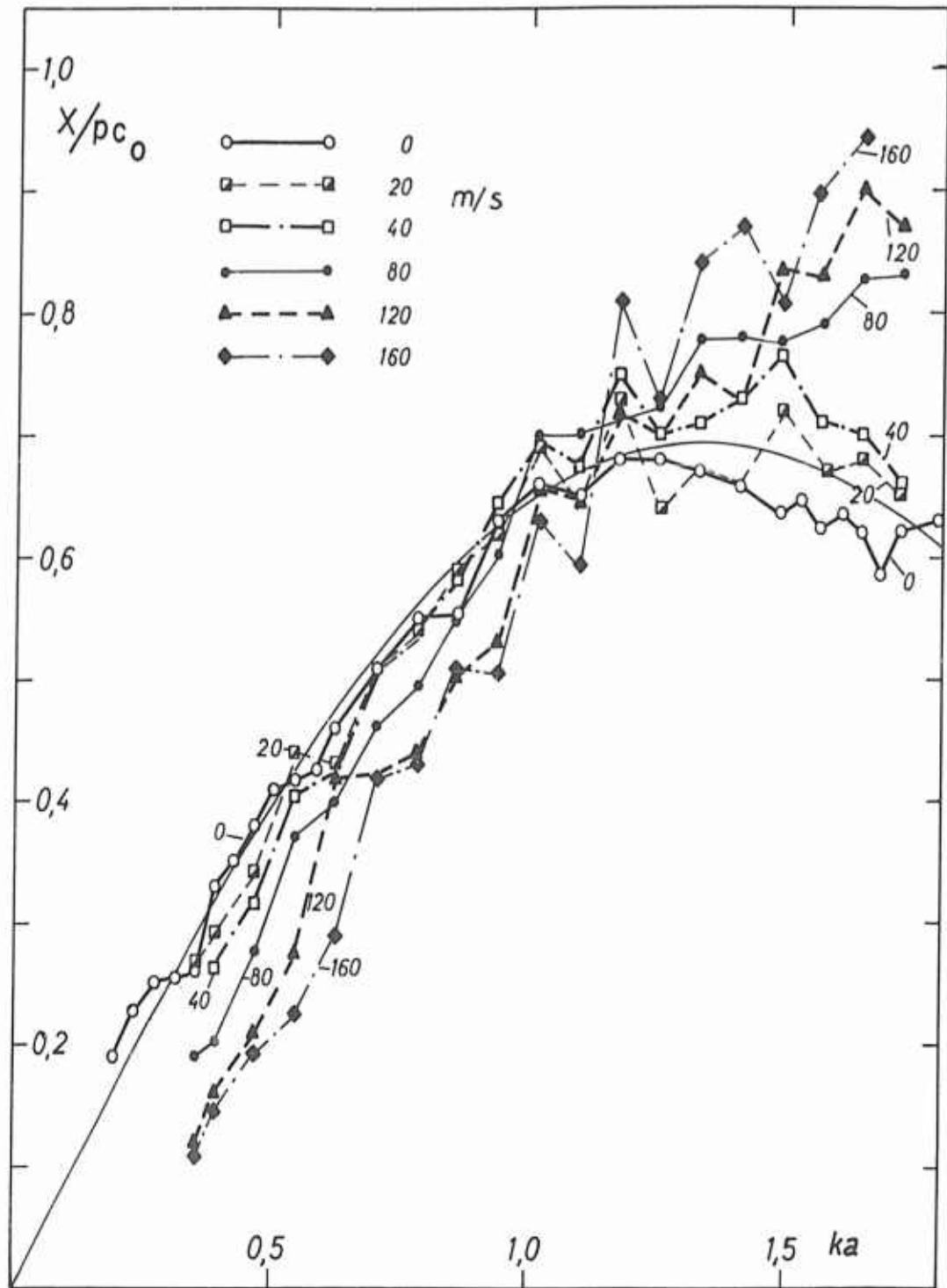


Figure 26 - Normalized imaginary part  $X/\rho c_0$  of the radiation impedance of the orifice in a baffle vs.  $ka$ . Parameter: Axial flow velocity  $V^1$ .

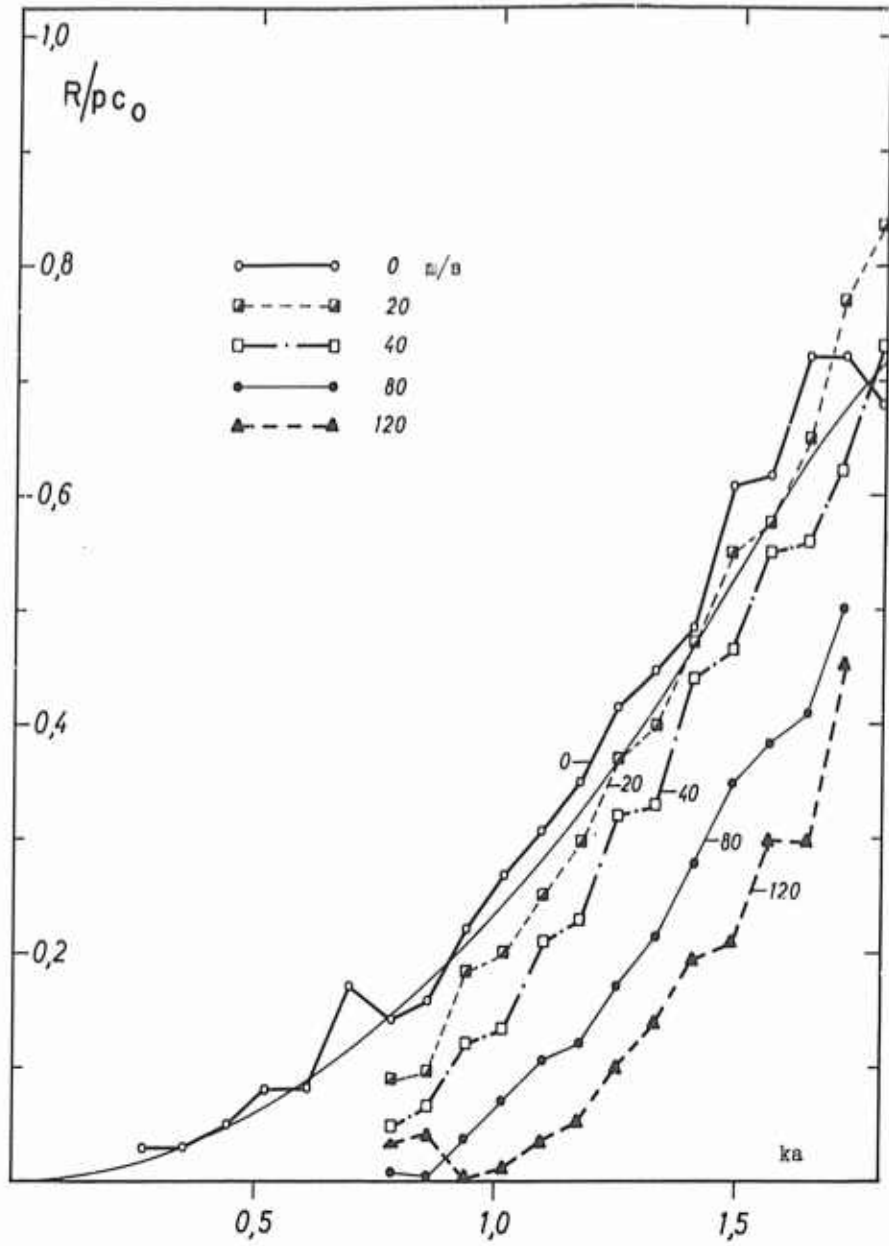


Figure 27 - Normalized real part of the radiation impedance of the unflanged orifice vs.  $ka$ . Parameter: Axial flow velocity  $V'$ .

#### IV. 2. Effects of Flow

The influence of the flow on the magnitude  $r$  of the reflection factor is clearly represented if the ratio  $r_M/r_0$  is plotted as a function of  $ka$ .  $r_M$  is the magnitude of the reflection factor with flow,  $r_0$  without flow. For great values of  $ka$  the experimental curves can be approximated by

$$\frac{r_M}{r_0} = 1 + A \cdot M \quad (12)$$

where the empirical value of  $A$  for the unflanged tube is  $A = 1.44$  and for the orifice in the baffle  $A = 1.67$ . The agreement with the measured values can be seen from Figure 23 where the Eq 12 is represented by the straight lines.

#### IV. 3. Effects of Obstructed Flow

Preliminary measurements have shown, that the turbulence in the orifice has a great influence on the impedance of the orifice. In these measurements two square rods, each 4 mm thick, were fixed across the orifice in the baffle. Without flow the rods had no influence on the impedance of the orifice. The impedance measured with the flow velocity of 80 m/sec coincided with the measurement at 30 m/sec without the rods. It seems as if the turbulence due to the rods would have decreased the change of the radiation impedance.

#### V. Measurement of the Reflection Coefficient of the Orifice with Increased Turbulence -

As stated above the reflection coefficient depends upon the turbulence degree behind the orifice. For the investigation of this effect different gratings were inserted into the orifice. The gratings are formed by concentric rings and radial bars of different number and different rod diameters. In Figure 28 a sketch of a grating (No. 5) is shown. In all measurements the discharge orifice was inserted in a large baffle.

Some measurements were made with a hot-wire anemometer for the determination of the turbulence level in the flow field behind the orifice for the axial flow velocity  $V_{\max} = 80$  m/sec. In Table I the average turbulence level in the core of the jet where the mean flow velocity is nearly constant are collected with some data about the gratings.

The coverage factor is the ratio of the area covered by the rods of the gratings to the orifice area.

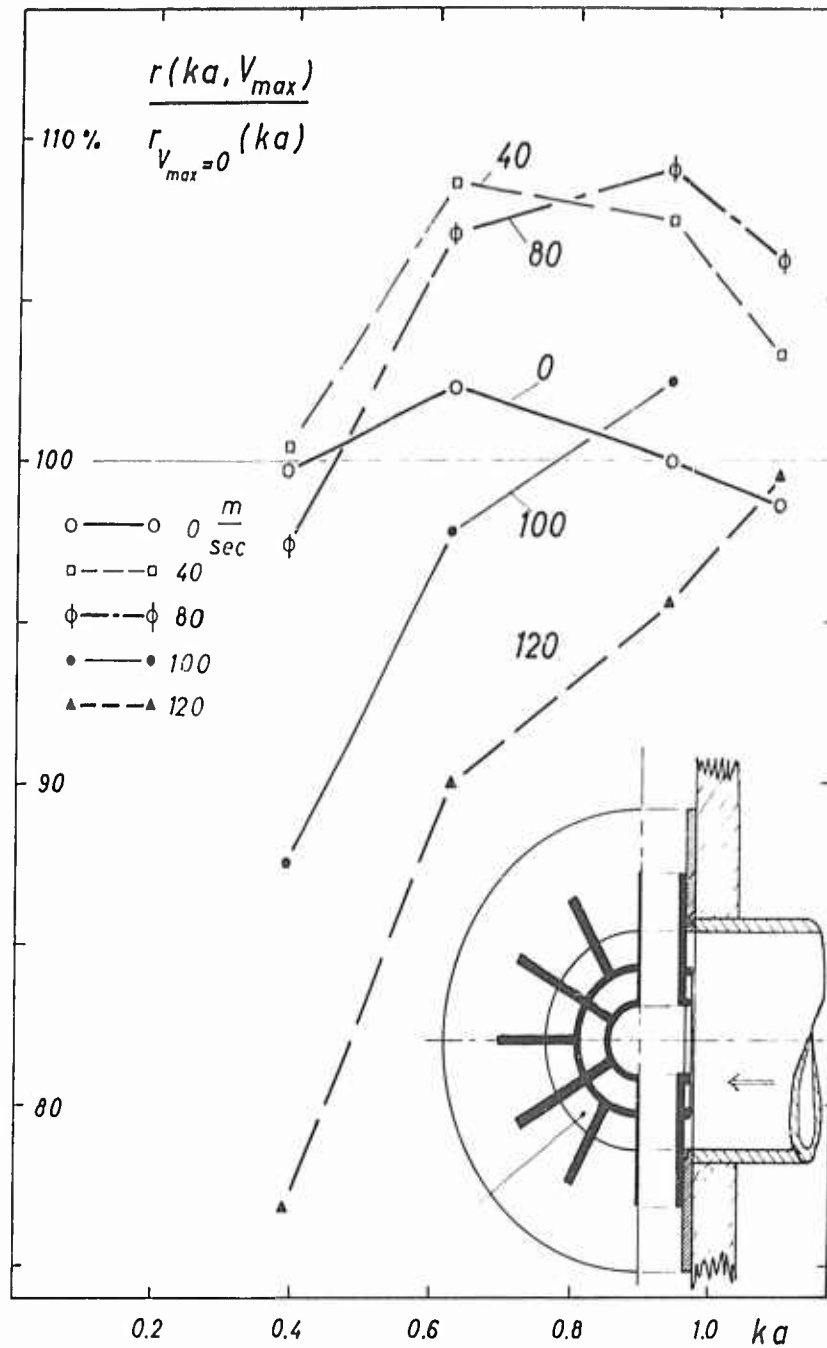


Figure 28 - Relative magnitude of the reflection coefficient of the orifice  $r(ka, V_{max})/r(ka, 0)$  vs.  $ka$ . Grating No. 5. Parameter: Flow velocity.

TABLE I  
AVERAGE TURBULENCE LEVEL IN THE CORE AS A FUNCTION  
OF GRATING PARAMETERS

	Free Orifice	Grating				No. 5
		No. 1	No. 2	No. 3	No. 4	
Rod diameter	---	2 mm				3 mm
Coverage factor	0	7 %	11 %	16 %	20 %	30 %
Turbulence level 5 cm behind the orifice $V_{\max} = 80 \text{ m/sec}$	5 %			8,7 %	7,6 %	12,6%

In a further set of measurements it was examined how the mean flow velocity field behind the orifice is affected by the gratings. The axial component of the mean flow velocity was registered by the hot-wire probe on passages across the jet at several axial distances from the orifice.

At a short distance from the orifice (5 cm) fluctuating velocity profiles are registered behind the gratings. At distances greater than 10 cm, however, the velocity profiles are almost the same with and without gratings.

The width of the jet behind the orifice is defined to be equal to the distance between the points of intersection of the tangents at the velocity profiles in the points of inflection with the abscissa. As it can be seen from Table II the insertion of the gratings has little effect on the width of the jet.

TABLE II  
WIDTH OF THE JET BEHIND THE ORIFICE IN CM  
TUBE DIAMETER 8.5 cm

Measuring Distance from Orifice	x = 10 cm	x = 20 cm	x = 100 cm
Free Orifice	10,4	13,2	29,6
Grating No. 3	10,8	14,4	29,0
Grating No. 5	10,5	14,4	31,2

Next, the reflection coefficient of the discharge orifice with the gratings was measured. The influence of the gratings on the reflection coefficient without flow was checked for the grating with the greatest coverage factor. By comparison with the measurements for the free orifice only small systematic differences, smaller than 5 per cent, were obtained. The reflection coefficient with flow  $r(f, V_{\max})$  was measured for several gratings.

In Figure 29 the dependence of  $r_f(V_{\max})$  from the flow velocity  $V_{\max}$  is shown for the constant frequency  $f = 1.2$  kcps. As previously shown for the free orifice the reflection coefficient depends linearly upon the flow velocity. In Figure 29 this dependence is represented together with the measured curves for some gratings. Almost all curves have the just mentioned straight line as a common tangent for  $V_{\max} = 0$ . For greater flow velocities the increase of the reflection coefficient with the gratings is smaller than without grating.

Since the gratings have nearly no influence on the reflection coefficient without flow nor on the distribution of the mean flow velocity the change of the reflection coefficient with flow can be ascribed to the change of the turbulence level. The greater the deviations are, the higher the turbulence level is. With the grating No. 5 the dependence of  $r_{1.2 \text{ kcps}}(V_{\max})$  from  $V_{\max}$  is only small (maximum deviation from  $r_{1.2 \text{ kcps}}(0)$  about 10 per cent). The curve for grating No. 5 indicates that it could be possible for higher frequencies that the reflection coefficient with flow could even be smaller than without flow.

In Figure 28 relative values of  $r(f, V_{\max})$  are presented for grating No. 5. It can be seen that the effect of the changed turbulence level increases towards lower frequencies. For the frequency  $f = 0.5$  kcps ( $ka = 0.39$ ) and high flow velocities the reflection coefficient becomes clearly smaller than without flow.

## VI. Conclusions -

The decrease of the real component of the radiation impedance due to the flow discharge is rather unexpected. In the flow field behind the orifice the flow velocity decreases from the axis of the discharge jet towards the outer regions of the jet. At least for high frequencies the thickness of the flow velocity gradient field is greater than the sound wavelength. One would have expected an outward refraction of the radiated sound and, as a consequence, an increase of the radiation resistance. The dependence of the sound radiation from an orifice upon the turbulence level could be of practical interest since in most practical cases the turbulence level in the jets behind discharge nozzles is rather high.

The measurements just reported reveal the importance of the turbulence level of the outflow. It will be the object of further measurements to show the relationship between the turbulence level and the degree of grid covering of the orifice. The effect of different shapes of the orifice will also be investigated.

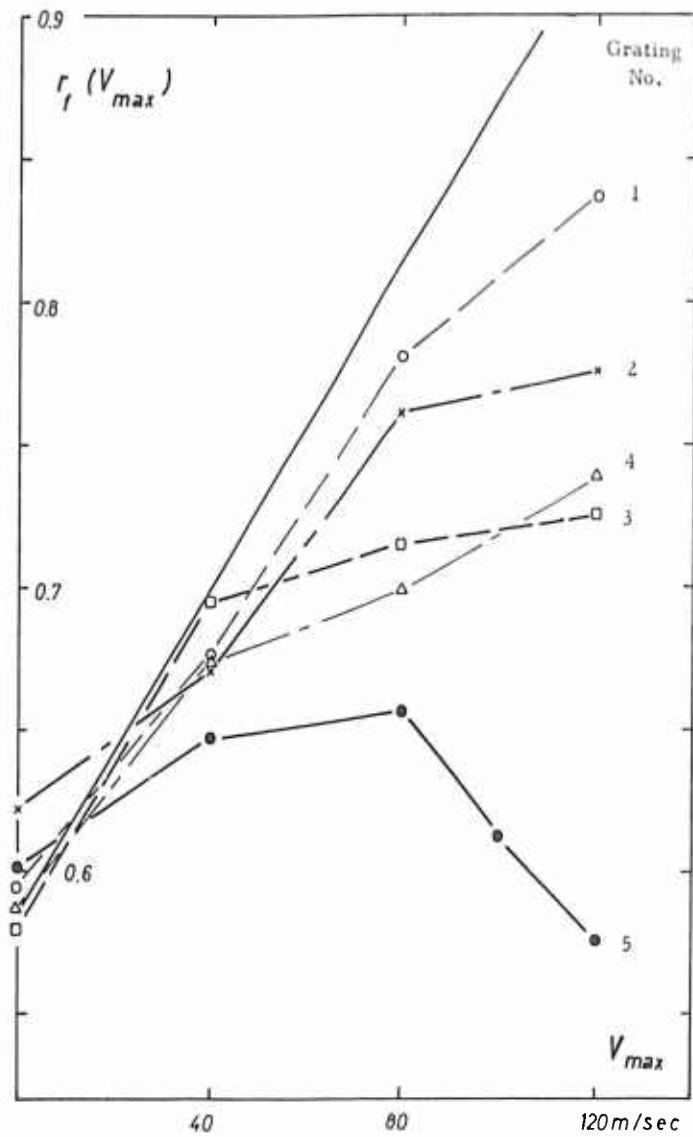


Figure 29 - Magnitude of the reflection coefficient of the orifice  $r_f(V_{max})$  at  $f = 1.2$  kcps for different gratings.



## REFERENCES

1. Kosten, C. W., "Die Messung der Schallabsorption von Materialien," (The Measurement of Acoustic Absorption of Materials), Proceedings of the Third International Congress on Acoustics, (German) Stuttgart, Vol 2, p 817, 1959.
2. Mechel, F. and P. Mertens, "Schallausbreitung in Absorbierend Ausgekleideten Stromungskanalen Bei Hohen Windgeschwindigkeiten" (Propagation of Sound in Absorbing Ducts at High Stream Velocities), Acustica, (German) Vol 13, No 3, pp 154, 1963.
3. Mechel, F., P. Mertens, and W. Schilz, Research on Sound Propagation in Sound Absorbent Ducts with Superimposed Air Streams, AMRL-TDR-62-140, Volumes I, II and III, 6570th Aerospace Medical Research Laboratories, Wright-Patterson Air Force Base, Ohio, December 1962.
4. Pridmore-Brown, D. C., "Sound Propagation in a Fluid Flowing through an Absorbent Duct," Journal of Fluid Mechanics, Vol 6, p 393, 1958.
5. Schlichting, H., Grenzschichttheorie (Boundary Layer Theory), Chapter XVI, Karlsruhe, 1958.
6. Schlichting, H., Grenzschichttheorie (Boundary Layer Theory), Chapter XX, Karlsruhe, 1958.
7. Schubauer, G. and H. Skramstad, Laminar Boundary Layer Oscillations and Transition on a Flat Plate, NACA Rep 909, NASA AFSS-AD Washington 25, D. C., 1948.